

Turbomachine Sealing and Secondary Flows

Part 3—Review of Power-Stream Support, Unsteady Flow Systems, Seal and Disk Cavity Flows, Engine Externals, and Life and Reliability Issues

R.C. Hendricks, B.M. Steinetz, and E.V. Zaretsky
Glenn Research Center, Cleveland, Ohio

M.M. Athavale and A.J. Przekwas
CFD Research Corporation, Huntsville, Alabama

The NASA STI Program Office . . . in Profile

Since its founding, NASA has been dedicated to the advancement of aeronautics and space science. The NASA Scientific and Technical Information (STI) Program Office plays a key part in helping NASA maintain this important role.

The NASA STI Program Office is operated by Langley Research Center, the Lead Center for NASA's scientific and technical information. The NASA STI Program Office provides access to the NASA STI Database, the largest collection of aeronautical and space science STI in the world. The Program Office is also NASA's institutional mechanism for disseminating the results of its research and development activities. These results are published by NASA in the NASA STI Report Series, which includes the following report types:

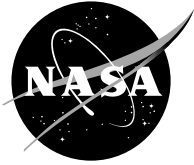
- **TECHNICAL PUBLICATION.** Reports of completed research or a major significant phase of research that present the results of NASA programs and include extensive data or theoretical analysis. Includes compilations of significant scientific and technical data and information deemed to be of continuing reference value. NASA's counterpart of peer-reviewed formal professional papers but has less stringent limitations on manuscript length and extent of graphic presentations.
- **TECHNICAL MEMORANDUM.** Scientific and technical findings that are preliminary or of specialized interest, e.g., quick release reports, working papers, and bibliographies that contain minimal annotation. Does not contain extensive analysis.
- **CONTRACTOR REPORT.** Scientific and technical findings by NASA-sponsored contractors and grantees.

- **CONFERENCE PUBLICATION.** Collected papers from scientific and technical conferences, symposia, seminars, or other meetings sponsored or cosponsored by NASA.
- **SPECIAL PUBLICATION.** Scientific, technical, or historical information from NASA programs, projects, and missions, often concerned with subjects having substantial public interest.
- **TECHNICAL TRANSLATION.** English-language translations of foreign scientific and technical material pertinent to NASA's mission.

Specialized services that complement the STI Program Office's diverse offerings include creating custom thesauri, building customized databases, organizing and publishing research results . . . even providing videos.

For more information about the NASA STI Program Office, see the following:

- Access the NASA STI Program Home Page at <http://www.sti.nasa.gov>
- E-mail your question via the Internet to help@sti.nasa.gov
- Fax your question to the NASA Access Help Desk at 301-621-0134
- Telephone the NASA Access Help Desk at 301-621-0390
- Write to:
NASA Access Help Desk
NASA Center for Aerospace Information
7121 Standard Drive
Hanover, MD 21076



Turbomachine Sealing and Secondary Flows

Part 3—Review of Power-Stream Support, Unsteady Flow Systems, Seal and Disk Cavity Flows, Engine Externals, and Life and Reliability Issues

R.C. Hendricks, B.M. Steinetz, and E.V. Zaretsky
Glenn Research Center, Cleveland, Ohio

M.M. Athavale and A.J. Przekwas
CFD Research Corporation, Huntsville, Alabama

National Aeronautics and
Space Administration

Glenn Research Center

Note that at the time of research, the NASA Lewis Research Center was undergoing a name change to the NASA John H. Glenn Research Center at Lewis Field. Both names may appear in this report.

Available from

NASA Center for Aerospace Information
7121 Standard Drive
Hanover, MD 21076

National Technical Information Service
5285 Port Royal Road
Springfield, VA 22100

Available electronically at <http://gltrs.grc.nasa.gov>

Turbomachine Sealing and Secondary Flows
Part 3—Review of Power-Stream Support,
Unsteady Flow Systems, Seal and Disk Cavity Flows,
Engine Externals, and Life and Reliability Issues

R.C. Hendricks, B.M. Steinetz, and E.V. Zaretsky
National Aeronautics and Space Administration
Glenn Research Center
Cleveland, Ohio 44135

M.M. Athavale and A.J. Przekwas
CFD Research Corporation
Huntsville, Alabama 35805

Abstract

The issues and components supporting the engine power stream are reviewed. It is essential that companies pay close attention to engine sealing issues, particularly on the high-pressure spool or high-pressure pumps. Small changes in these systems are reflected throughout the entire engine. Although cavity, platform, and tip sealing are complex and have a significant effect on component and engine performance, computational tools (e.g., NASA-developed INDSEAL, SCISEAL, and ADPAC) are available to help guide the designer and the experimenter. Gas turbine engine and rocket engine externals must all function efficiently with a high degree of reliability in order for the engine to run but often receive little attention until they malfunction. Within the open literature statistically significant data for critical engine components are virtually nonexistent; the classic approach is deterministic. Studies show that variations with loading can have a significant effect on component performance and life. Without validation data they are just studies. These variations and deficits in statistical databases require immediate attention.

Keywords: Turbomachine, seals, secondary flow, engine externals, component life

Introduction

Many components in today's turbomachines were designed "on the boards" by competent, knowledgeable engineers based on sound fundamentals. Although standard in the past, this practice is rapidly yielding to component solid modeling with the designer able to access interfacing components and perform some degree of optimization, including material selection and stress analyses. In many respects the designer knows more and has more information at each stage of the design but in other ways often lacks the hands-on knowledge and competency of the seasoned engineer. There is no substitute for in-field experience and feedback data. Further, we are rapidly approaching performance limits in terms of what can be accomplished through "material bending," and unsteady fluid flows are becoming the next performance challenge.

Turbomachine sealing and cavity flow problems are unsteady in nature owing to the blade/vane interaction of the rotating system, and the challenge becomes how to best analyze and use these flows. Validated tools must be developed to assist the designer and engineer with steady and unsteady flow and heat transfer issues relating to power-stream and overall engine performance. For example,

multiply-connected cavities with conjugate heat transfer must be considered in detail when seeking small percentage gains in component efficiency. It is equally important to account for disk and blade or vane cooling and purge flows because small changes in thermal and flow characteristics effect large changes in engine life and can degrade engine performance. Most of these flows are controlled by compressor or pump bleeds through fixed orifices, but many are controlled through seals, valves, pipes, and controllers, constituting a small portion of the engine externals.

Engine externals, all the “stuff” hanging on the engine case, are too often neglected in a research program. However, without engine externals the engine simply will not operate. Because the complexity of the externals space does not lend itself readily to modeling, one resorts to experiment, even for such critical functions as fire prevention. Nevertheless, engine externals account for a large percentage of the day-to-day maintenance problems and influence engine life.

Maintenance intervals and component lifing are critical issues to both the astronauts and the traveling public. The airlines and NASA work very hard to ensure safety and component reliability. Nevertheless, component design life is still established through testing and history, and improvements in lifing methods are both necessary and continually sought.

In part 1 we review some sealing requirements and limitations from the viewpoints of the customer, designer, and researcher along with marketing forces. In part 2 we explore turbomachine sealing dynamics methods and computational and numerical modeling. Herein, we address the issues of multiply-connected cavities with conjugate heat transfer, the nature of compressor and turbine blade flows, and the interaction and complexity of engine externals and illustrate some facets of component lifing.

Unsteady Flow Systems

As cited in part 2, turbomachines are unsteady systems that induce unsteady loadings into the bypass (fan) and the power and the secondary flow streams. In addition, each stage of the fan, compressor, and turbine cavities must be pressure and load balanced on one, two, or three spools. Usually, one considers a gas-generator spool, or high spool, and a power spool, or low spool. However, each manufacturer optimizes to produce the best power, economy, and environmental ratings for the cost.

As an example of air-breathing turbomachines the NASA Energy Efficient Engine (E³) has a T1 turbine (first stage of the high-pressure turbine) with 76 blades and 46 stators. The objective is to produce hot, high-pressure gas to drive the high-pressure compressor. The low-pressure turbine powers the low-pressure compressor and fan. These systems require long life and high reliability. Thus, rapidly pulsing combustion gases must be kept from the cavities and confined to the blade platform regions without reingestion into the turbine or compressor flow streams, which degrades performance. Also, unsteady blade tip flows must be controlled with minimal losses, thus preventing separating, flow passage blockage, stall, or unstart. In addition, the interface purge and cooling air must be properly metered and sealed to provide load balancing.

Rocket engine turbomachines have similar interfacing and load-balancing problems, but the flight profile requirements are more severe. Combinations of cryogenics, rapid startup, high rotor speeds, propellant-lubricated bearings, very high strength/weight ratio components, and dynamics are sealing and secondary flow design challenges. Looking ahead, valved and valveless pulse and continuous-wave detonation engines being developed are unsteady devices that present yet another set of sealing challenges to contain reflected shocks and maintain proper inlet pressures within the combustion tube.

Seal and Disk Cavity Flows

Although this is by no means intended as a comprehensive review, we will highlight a few important findings. A considerable amount work has been performed on fluid flow and heat transfer mechanisms in cavities formed within rotating and stationary disks. Figure 1 shows a typical multistage turbine cavity section. Several experimental studies have been reported that consider both simplified and complex disk cavity configurations (e.g., Chen, 1991; Chew et al., 1988, 1992; Graber et al., 1987; and Johnson et al., 1991, 1994).

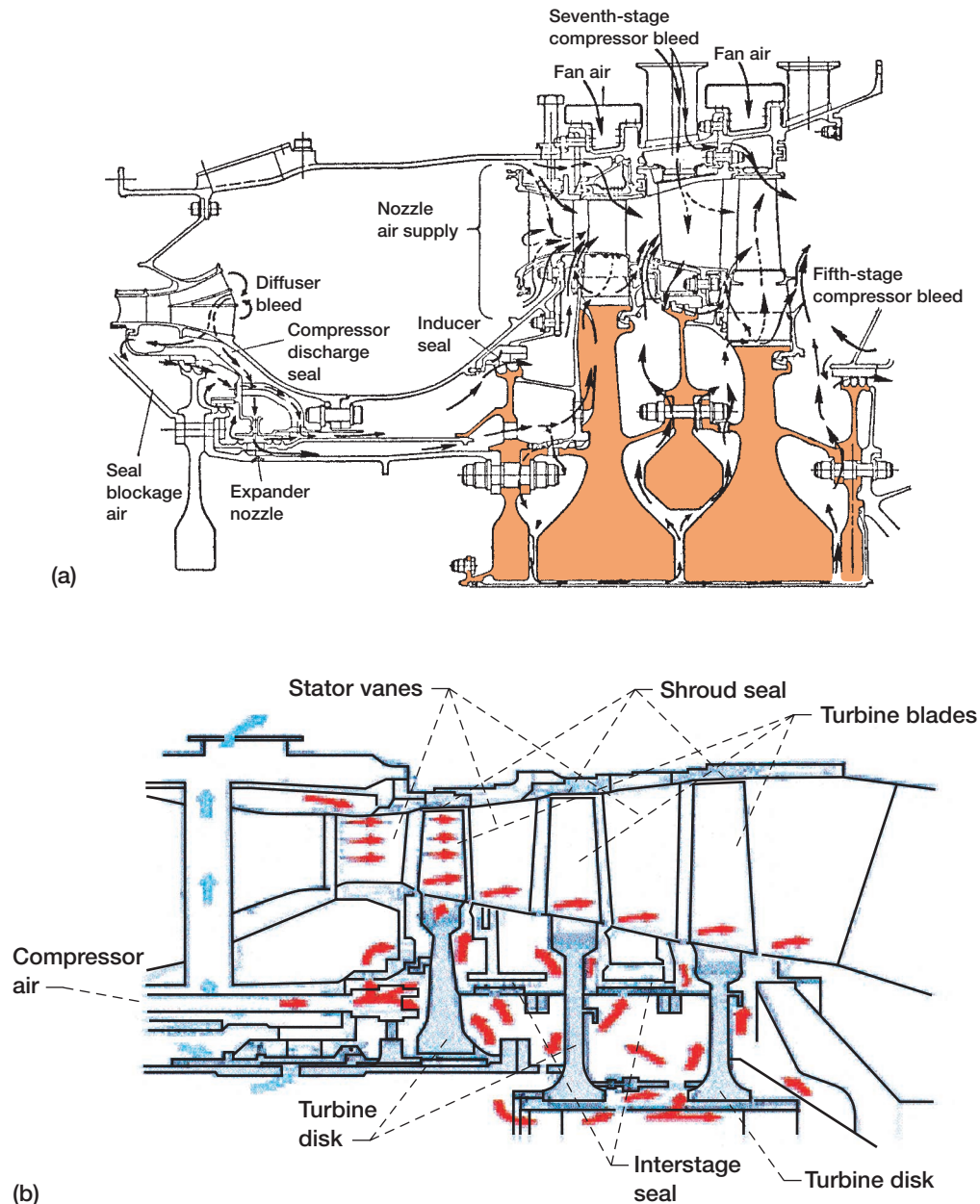


Figure 1.—Typical multistage turbine cavity section. (a) Energy Efficient Engine high-pressure turbine (Halila et al., 1982). (b) Hypothetical turbine secondary-air cooling and sealing (Allcock et al., 2002). Courtesy AIAA. See also figures 13 and 5 of part 1.

Hendricks et al. (1995) set forth a comprehensive review of secondary flow system developments with the power stream in aerospace components for the NASA seals and secondary flow system codes SCISEAL and INDSEAL. These development efforts are also tracked in the NASA Seals Code and Secondary Flow Systems Development publications (1991 to present). The coupling of the power-stream flows with seals and cavity flows is a necessary aspect of multistage compressor and turbine design. Athavale et al. (1997, 1998) have reported detailed descriptions of these tools and representative simulations. (See also Janus et al., 1989, 1992.)

These works include the gas-path flows through the stages (blades and vanes) and those under the platform cavity and in the sealing region. The interaction between these two flow streams significantly affects performance. The tip sealing (shroud/rotor and interstage/stator interfaces) is equivalently important and can be handled in a similar manner. However, for this discussion we will confine our attention to the region between the shaft and the blade or vane platforms. The interstage/labyrinth/rim seal interface design, locations, and requirements differ between the compressor and the turbine. For example, on the compressor side the goals are to keep leakage small, to reduce windage, and to mitigate the reintroduction of flow into the gas path. On the turbine side, the goals are to reduce losses and to prevent gas-path ingestion with careful attention to rim sealing (fig. 1).

Teramachi et al. (2002) investigated rim interface sealing (figs. 2 and 3), providing data and some computational fluid dynamics (CFD) results on four rim seal configurations: (0) T-on rotor, (1) T-on rotor with overlap T-on stator, (2) T-on stator with overlap T-on rotor; and (3) fish mouth on rotor with overlap T-on stator. Dummy stators were introduced, but there were no blades on the rotor. Carbon dioxide concentration measurements (similar to the work of Bruce Johnson (Graber et al., 1987)) defined seal effectiveness in terms of the ratio of purge gas to ingested gas. Figure 4 shows the experimental effectiveness of these configurations, where flow coefficient $C_w = Q/vb$ and $Re_m = Vb/\nu$, where b is the cavity outer radius, V the mean flow speed, Q the purge flow rate, and ν the kinematic viscosity. Configuration (3) is the least affected by changes in overlap and configuration and (0) the most; configuration (2) is quite sensitive to overlap. The high effectiveness of

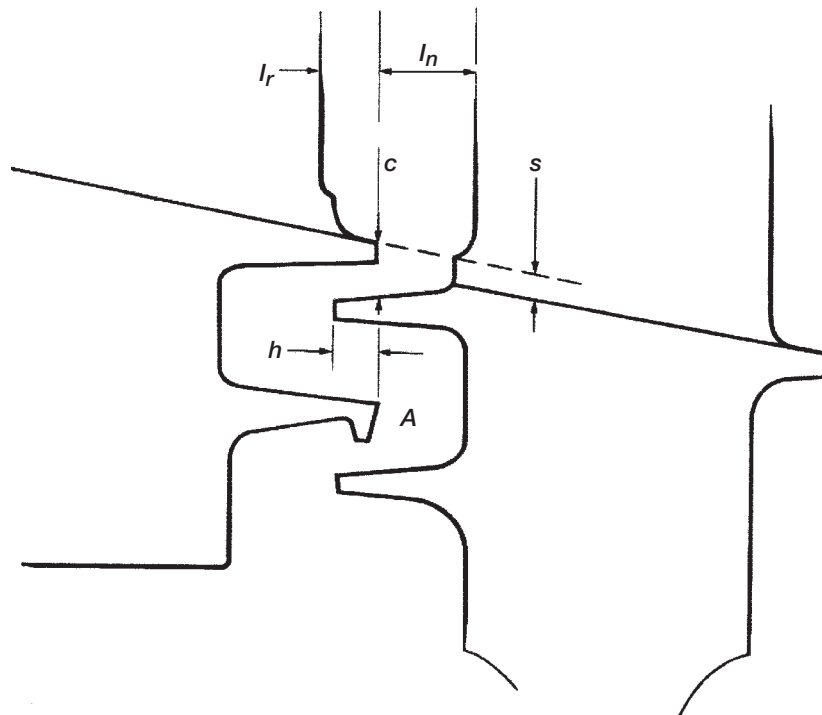


Figure 2.—Generic turbine nozzle rotor gap configuration. (Campbell, 1978). See also figure 7 of part 1.

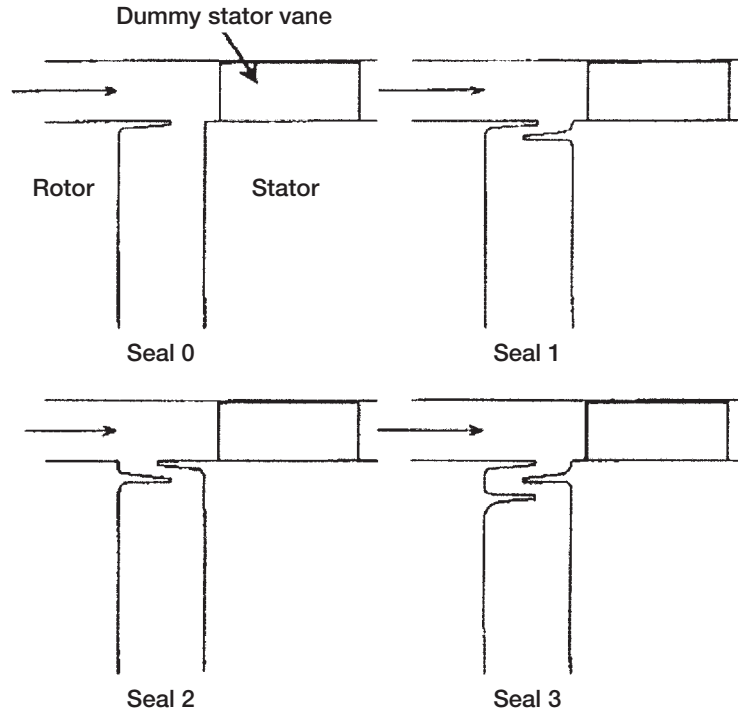


Figure 3.—Experimental rim seal configurations. (Teramachi et al., 2002.) Courtesy AIAA. See also figure 37 of part 1.

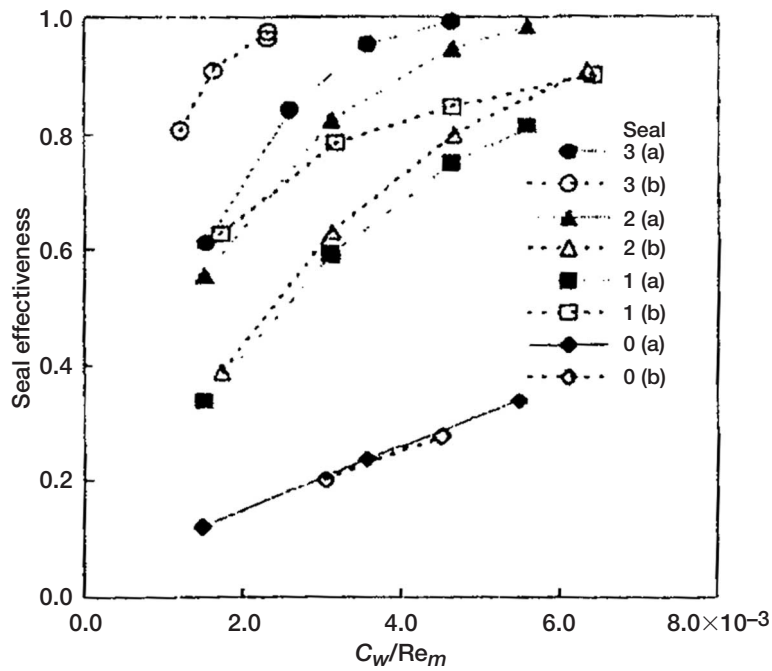


Figure 4.—Comparison of experimental rim seal data at Reynolds numbers (a) 2.4×10^6 and (b) 1.1×10^6 . (Teramachi et al., 2002.) Courtesy AIAA.

configuration (3) is related to the buffer cavity between the two rotor seal teeth with a stator tooth between the rotor teeth. The lowest effectiveness of configuration (1) is due to the large clearance gap, although the ingestion is nearly zero. A CFD code jointly developed by the National Aerospace Laboratory–Japan and the University of Manchester’s Institute of Science and Technology (turbulent, k - ϵ , with wall functions) was applied to these configurations. The results show the gap recirculation zone where power-stream gas is ingested at on-pitch positions and ejected at midpitch positions (i.e., flow ingestion at the vane leading edge partially returns in the midpitch region mixing with the purge air; see also Wellborn and Okiishi, 1996). Athavale et al. (1999) in studying the Allison 501D turbine found that ingested fluid could work its way well into the disk space, even though purge fluid flows were substantial.

Wellborn and Okiishi (1996, 1999) investigated the effect of leakage in a four-stage, low-pressure compressor with blading design based on the NASA E³ engine. Figure 5 illustrates the NASA Glenn low-speed, axial-flow compressor’s (LSAC) stage 3 cavity geometry. For the configuration tested there was a monotonic decrease in performance with increased leakage but no observable effect on stall margin. Variations in performance due to seal leakages were localized at the bottom 0.4 of span, but there was a region of blockage near the hub due to recirculating leakage flow. Flow was injected into the power stream near midpitch of the upstream cavity and sucked into the cavity near the blade stagnation point. Flow is into the cavity over most of the downstream cavity, with localized ejection near the stator wakes. Here, low tangential or axial momentum in the upstream cavity degraded the suction-side boundary layer. Seal leakages did not affect upstream stages but did progressively degrade performance of the downstream stages. For each 1 percent change in clearance/span ratio the pressure rise penalty was nearly 3 percent with a 1-percent drop in efficiency. Hall and Delaney (1993a,b, 1995) simulated the LSAC experiments with Adamczyk’s ADPAC analysis package. (They also completed sensitivity studies but did not address the effects on rotordynamics.)

Very few studies on the full-time, accurate interaction of nonaxisymmetric flow on the rim seal are available. Heidegger et al. (1996) presented three-dimensional solutions of the interaction between the power stream and seal cavity flow in a typical multistage compressor (fig. 6). Using the Allison/NASA-developed ADPAC code, they performed a parametric study on a three-tooth labyrinth seal/cavity configuration (fig. 7) and a sensitivity study to various sealing parameters (fig. 8). Figure 9 nicely images a class of generic labyrinth seal tooth geometries. Their study shows

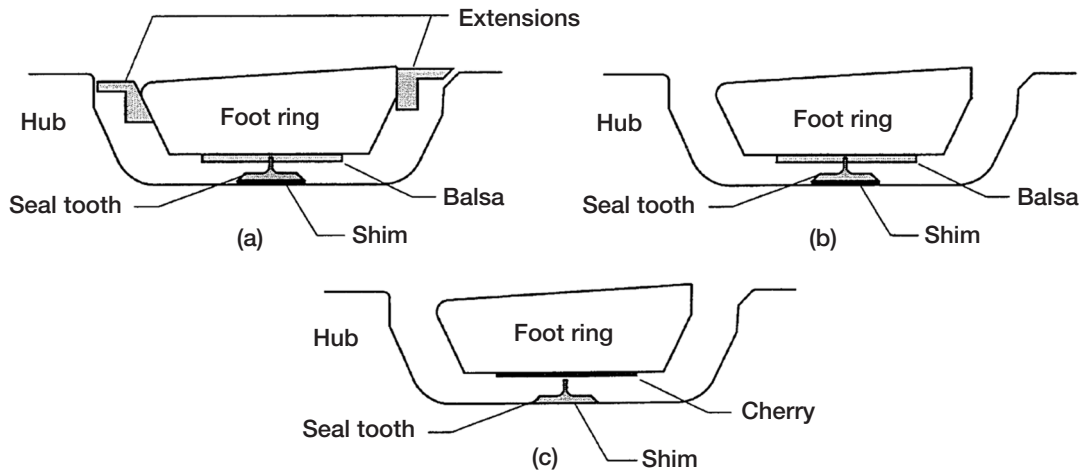


Figure 5.—Illustrations of low-speed compressor shroud sealing configurations at rotor (hub)/stator interface. (a) No cavity with nominal zero leakage. (b) Minimum-leakage cavity. (c) Baseline cavity; intermediate and maximum leakage with clearance changes. (Wellborn and Okiishi, 1996.) See also figures 6 and 7.

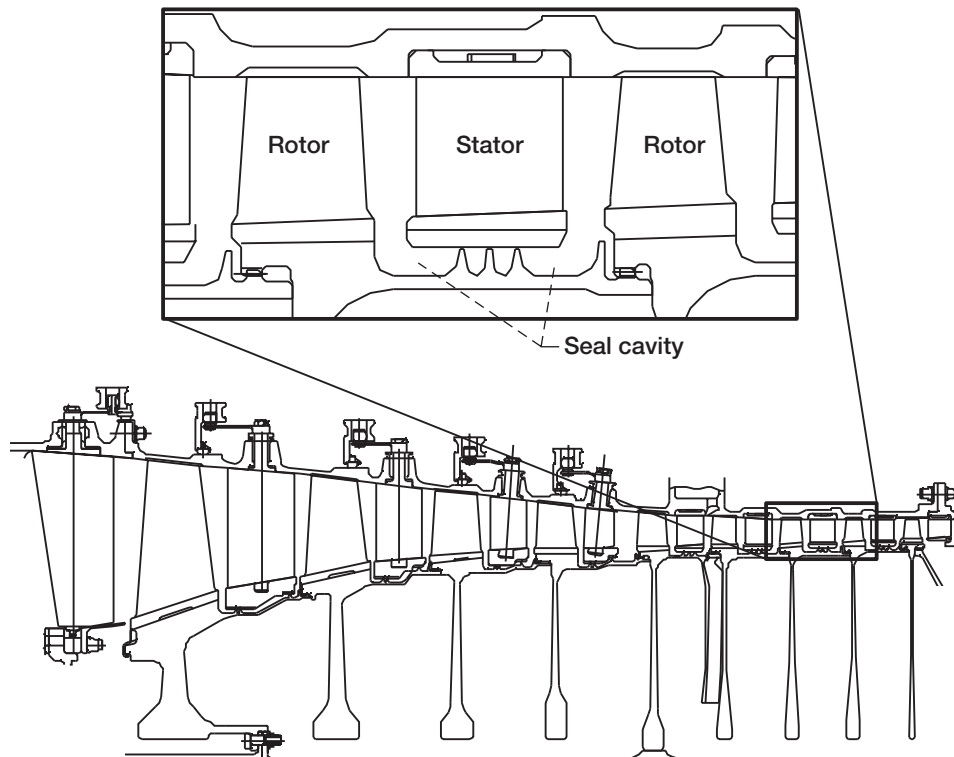


Figure 6.—Schematic of typical high-speed axial compressor with closeup view of seal cavity region under inner-banded stator. (Heidegger et al., 1996.)

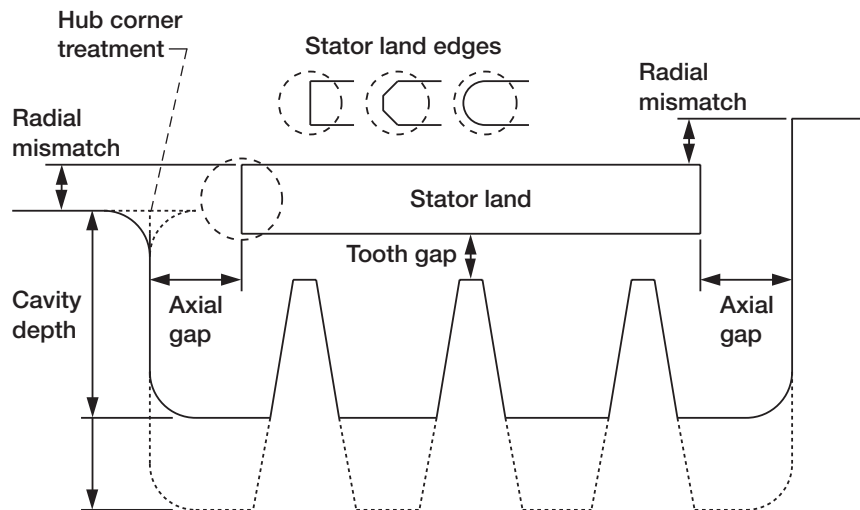


Figure 7.—Geometric parameters defining overall seal/cavity geometry. (Heidegger et al., 1996.) See also figure 38 of part 1.

that the leakage flow out of the seal cavities can affect the power stream significantly, mainly by altering the inlet flow near the stator blade root area, and can potentially affect the performance of the overall compressor (fig. 10). Feiereisen et al. (2000) completed an experimental study of the primary and secondary flow in a turbine rig. It represents a first attempt at understanding this interaction and at generating data for validation.

CFD techniques are increasingly being used to provide detailed flow field information on more complex cavity shapes and complex flow phenomena that cannot be treated with analytical methods. Several studies on single-cavity configurations with simplified geometry have been reported (e.g., Athavale et al., 1992; Chew, 1988; and Virr et al., 1994). The cavities considered in these studies were of the rotor-stator type with a rim seal and coolant injection. Some measure of interaction with main-path flow was provided. As noted in figures 1 and 6, an engine has multiple, linked disk cavities, with complex shapes including bolts and holes. CFD techniques provide a way to account for the complex interaction in such configurations, but even then simplifications are required. Several studies on complete turbine drum simulations have been reported (Athavale et al., 1995; Ho et al., 1996).



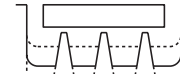




Parameter	Baseline case	Variations
Seal tooth gap	0.010 in.	 No cavity, no gap, 0.020 in., 0.040 in.
Wheel speed (rpm)	100%	 58% baseline speed
Seal cavity depth	0.184 in.	 $\pm 50\%$ of baseline cavity depth
Radial mismatch of hub flow path: Upstream Downstream	0.000 in. 0.000 in.	 $\pm 5\%$ stator span $\pm 5\%$ stator span
Axial trench gap: Upstream Downstream	0.081 in. 0.061 in.	 $\pm 20\%$ of baseline gap
Hub corner treatment: Leading edge Trailing edge	Sharp Sharp	 Rounded back Sharp Rounded forward
Stator land edge treatment	Faceted	 Faceted Rounded

Figure 8.—Test matrix of geometric parameters to be tested relative to baseline configuration. (Heidegger et al., 1996.) See also figure 39 of part 1.

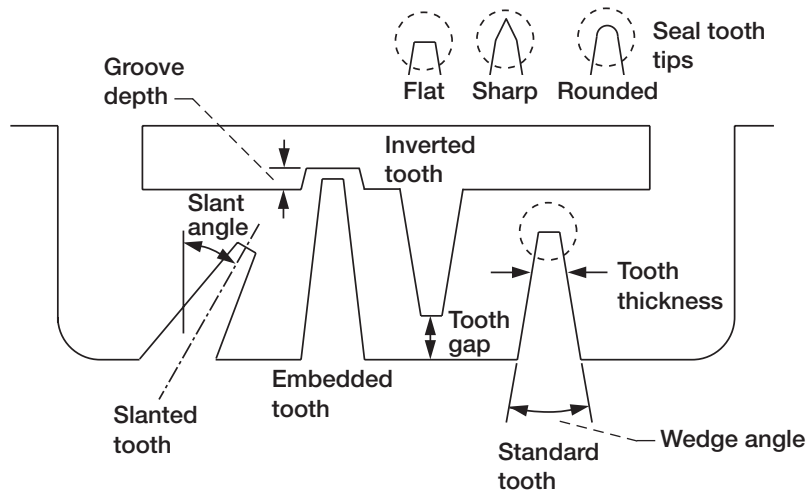


Figure 9.—Geometric parameters defining individual and generic seal tooth geometries. (Heidegger et al., 1996.) See also figure 40 of part 1.

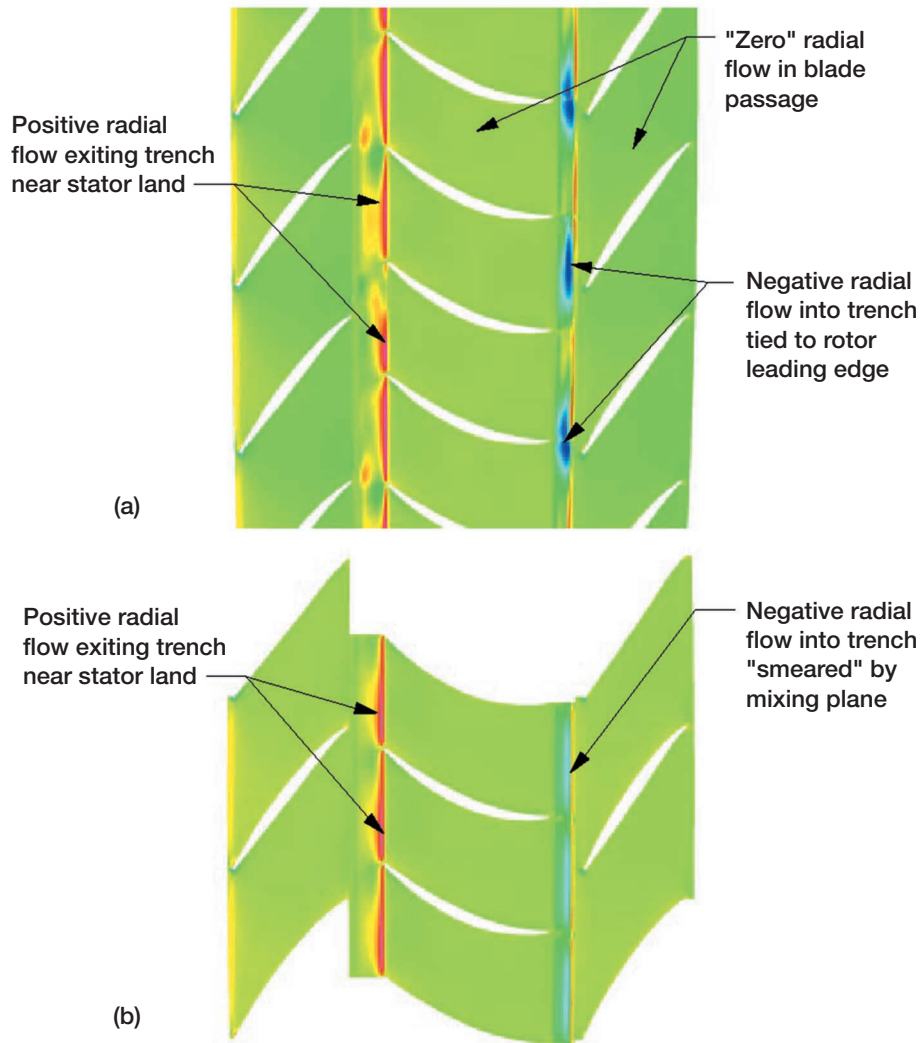


Figure 10.—Contours of radial velocity located one computational cell above hub (rotor) surface for coarse mesh. (a) Unsteady and (b) mixing-plane rotor/stator ADPAC solutions. (Heidegger et al., 1996.)

In the treating coupled flows consider where and when model simplification can be used. Often two-dimensional or steady-state flow and heat transfer can be used as opposed to a complete conservative three-dimensional transient with fully coupled interactions including conjugate heat transfer. However, conjugate heat transfer is important in calculating disk temperature distributions. For example, as figures 11 to 14 show, the calculated interaction between power-stream and secondary flows would not match the Allison 501D turbine results without conjugate heat transfer (Ho et al., 1996; Athavale et al., 1999). Conjugate heat transfer is most important in determining the T1-rotor platform temperatures, especially at the power-stream interfaces where the thermal gradient from the platform to the hub is significant. These aerothermomechanical loads can drastically affect disk and engine life, as discussed later. (It is also important to include geometric deformation. Because deformation is not yet a part of SCISEAL, a separate finite element analysis code must be used.)

So the objectives are to develop a simulation methodology for coupled solutions of the power-stream and secondary flow fields considering (1) transient, coupled two-dimensional simulations, extending the NASA seals and secondary flow systems code and (2) “steady-state” simulations for quick-turnaround preliminary designs that can be interfaced and augmented with the NASA seals code INDSEAL. Either method requires both time-accurate and steady-state validation against available data, followed by extensive beta testing of the codes and feedback by the original engine manufacturers (OEM’s). For the transient coupled simulations the code SCISEAL for below-platform flows is coupled with MS-TURBO for power-stream flows. These codes treat the flow physics differently, requiring special information transfer techniques at the interface. SCISEAL is a pressure-based, turbulent, heat-and-mass-transfer (including conjugate), slower-flow code. MS-TURBO is a density-based, unsteady, rotor-stator interactive, fast-flow code. At the interface the primitive variables of SCISEAL are passed to MS-TURBO, and the primitive variables of the

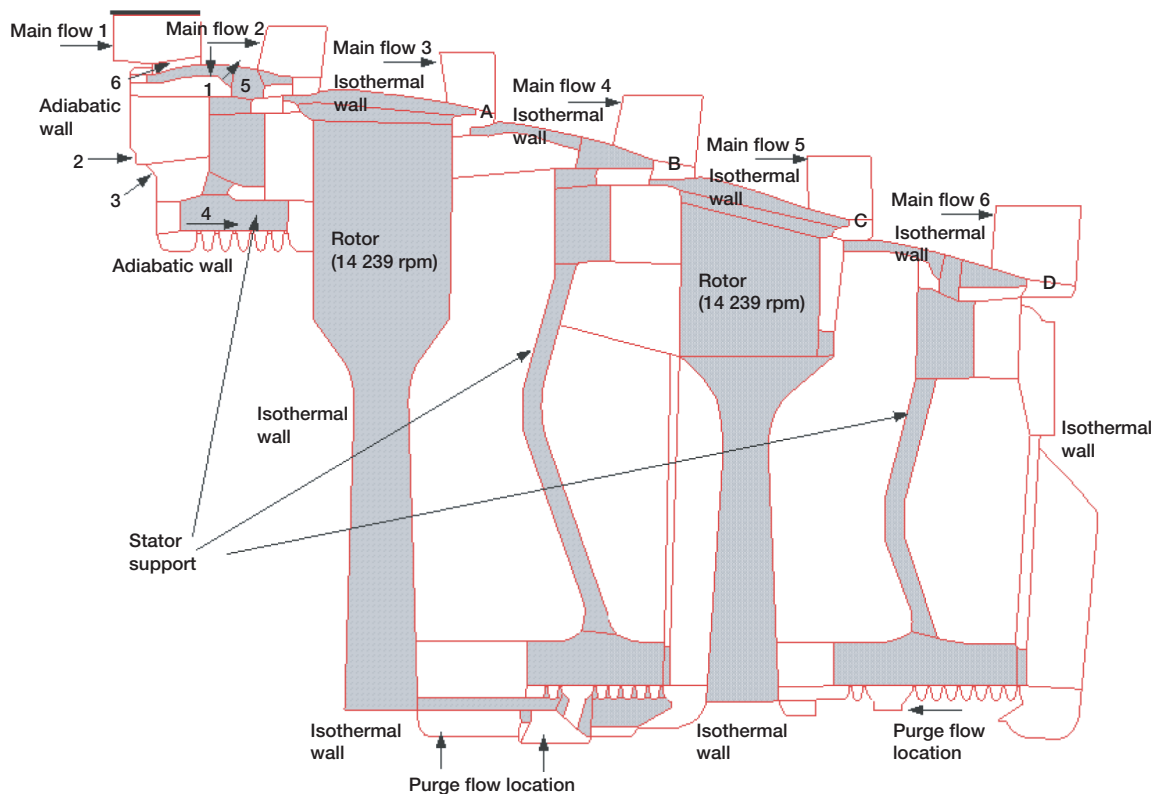


Figure 11.—Flow domain and conditions for conjugate heat transfer calculations of all inner disk cavity pairs. Shaded areas denote conjugate heat transfer. Static pressures are specified at six main flow exits. (Athavale et al., 1999.)

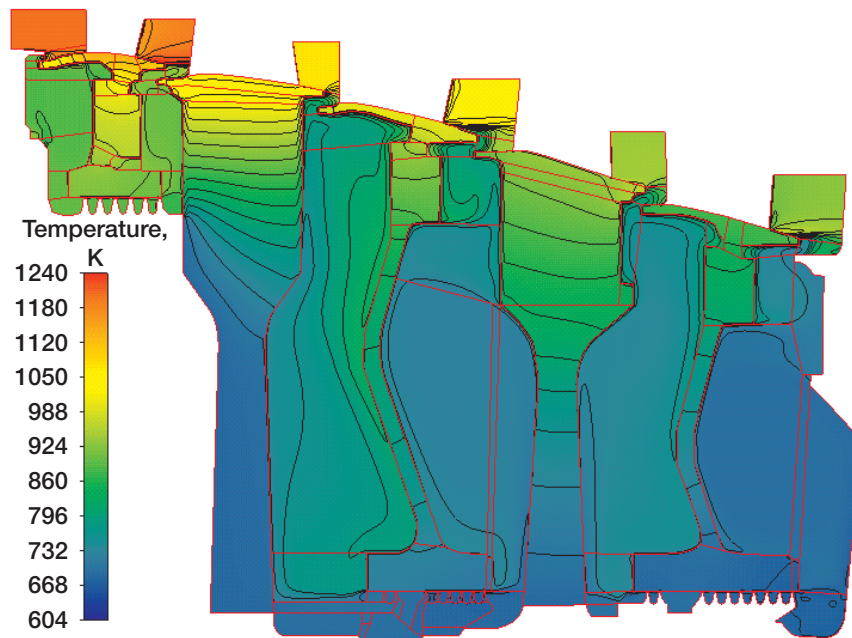


Figure 12.—Temperature field in fluid and solid parts of turbine cavities (absolute frame). (Athavale et al., 1999.)

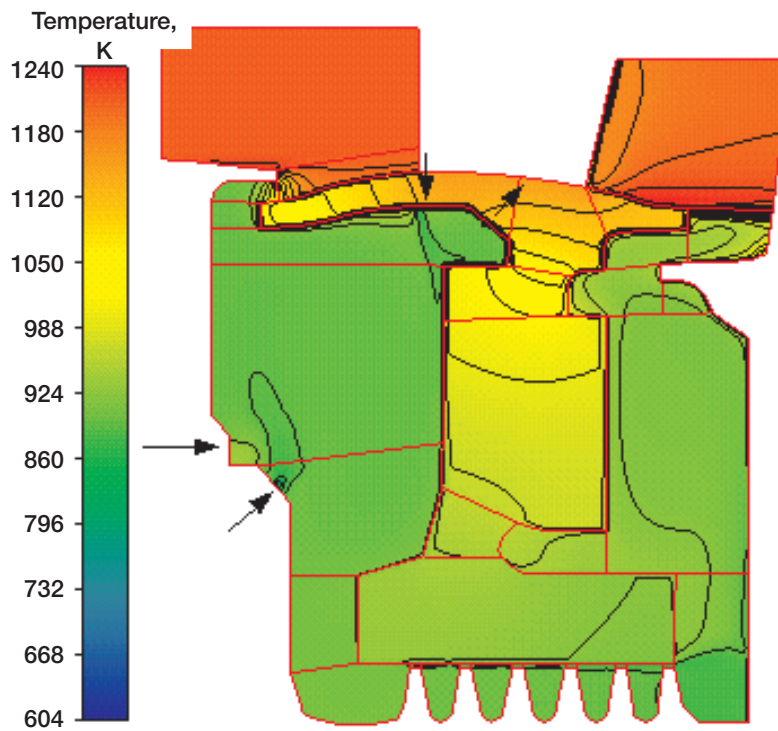


Figure 13.—Details of streamlines and temperatures in stage 1-2 cavities with conjugate heat transfer (absolute frame). (Athavale et al., 1999.)

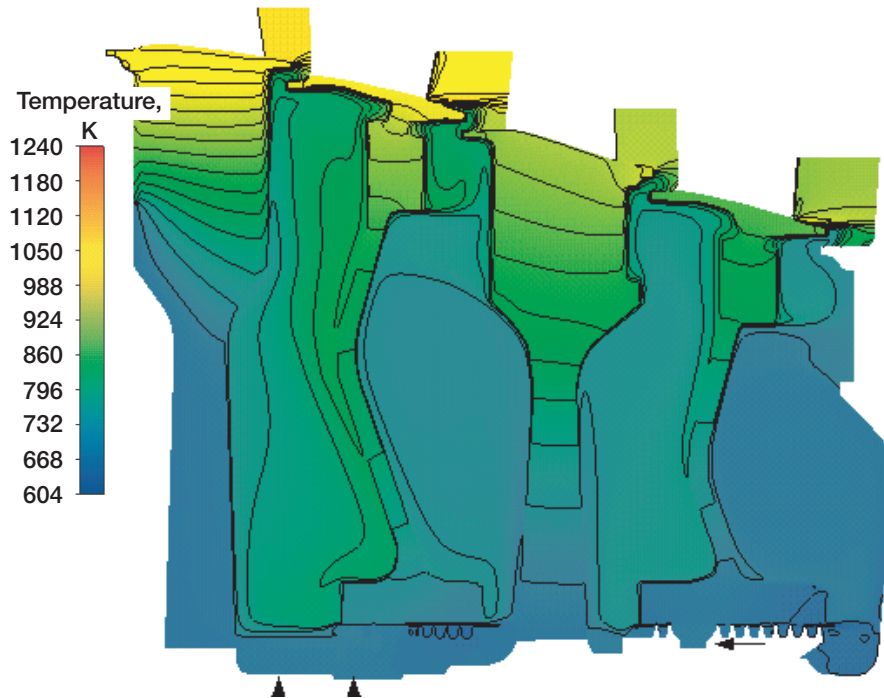


Figure 14.—Stream function and conjugate heat transfer temperature fields in stage 2-3 and 3-4 cavities (absolute frame). (Athavale et al., 1999.)

MS-TURBO boundary ghost layer are used to calculate interface fluxes. These fluxes are then passed to SCISEAL as the interface boundary conditions, ensuring continuity of fluxes across the interface, while TURBO controls the time steps requiring proper code synchronization to transfer data files (fig. 15).

To minimize solution times, SCISEAL could be used to treat both the power-steam and below-platform flow as was done by Heidegger et al. (1996) with the Allison/NASA-developed ADPAC code. The time dependency of relative motion issues would be resolved, but circumferential averaging for the sliding interfaces would be required (fig. 16). Using SCISEAL would provide a fast way of assessing a particular design, allowing treatment of complex cavity-rim configurations and near-term optimization, and would serve as the starting point for the time-accurate calculations using the coupled SCISEAL and MS-TURBO codes. (This single-code SCISEAL procedure, three-dimensional at the mixing plane in the power stream and two-dimensional in the cavity, for steady-state calculations is still in the process of being finished.)

The coupled codes SCISEAL and MS-TURBO (Athavale et al., 2001) have been applied to several experimental test rig data sets showing conditions under which ingested flow can be controlled. Consider the configuration illustrated in figure 17 and its associated computational grid (fig. 18). Athavale applied the code to the 30° pi-sector with four vanes (stators) and five blades (rotors) simulating the stator/rotor set (48/58) of Feiereisen et al. (2000), with a three-tooth labyrinth seal and overlap rim seals. The stator grid is 49 axial by 12 radial by 15 circumferential (tangential); the rotor grid is 36 by 12 by 12, a coarse grid. The interface zone is 8 axial by 60 circumferential (tangential) for the power stream and 8 by 30 for the cavity. The TURBO code (the version employed in the study) did not have the k - ϵ turbulence model, and the boundary values at the interface had to be inferred or estimated from the presumed rim seal solution. The interface values of k and ϵ affect the turbulent viscosity in the critical flow area of the rim seal. Improper specification of the k - ϵ values at the interface destabilized the solution at low purge flow rates. The calculation procedure immediately stabilized after reasonable values of turbulent parameters were used at the rim seal interface.

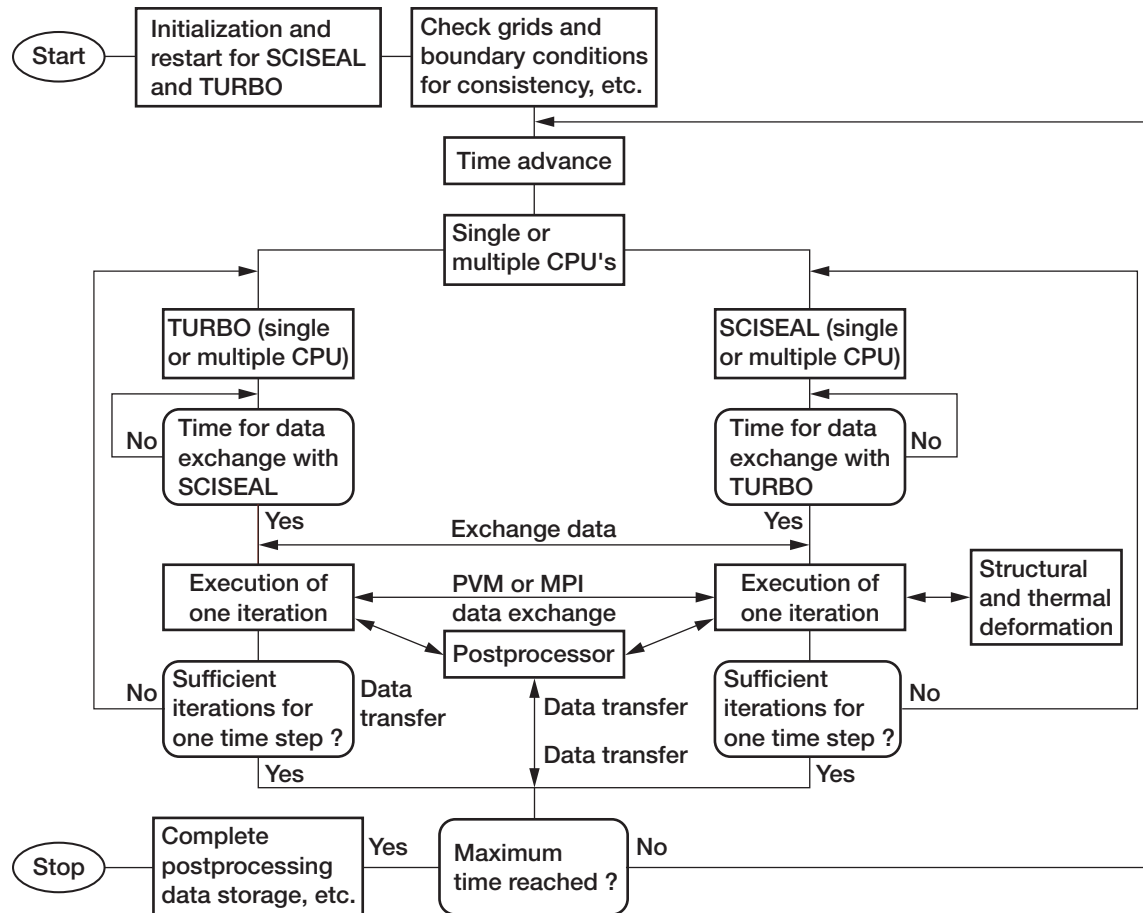


Figure 15.—Flow schematic for coupled execution of SCISEAL and TURBO codes. (Athavale et al., 2001.) PVM (parallel virtual machine); MPI (message passing interface).

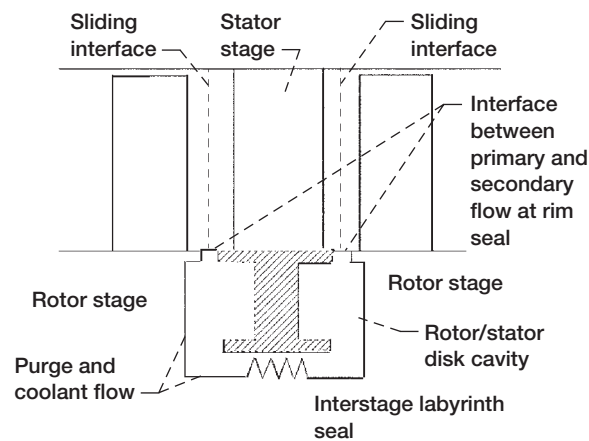


Figure 16.—Schematic of a typical interstage cavity configuration with sliding interface boundary condition. (Athavale et al., 2001.)

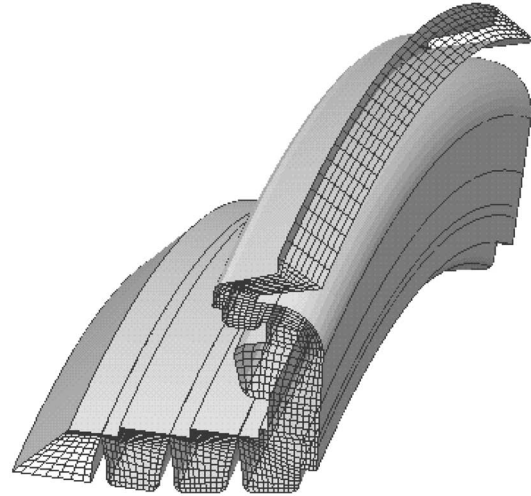
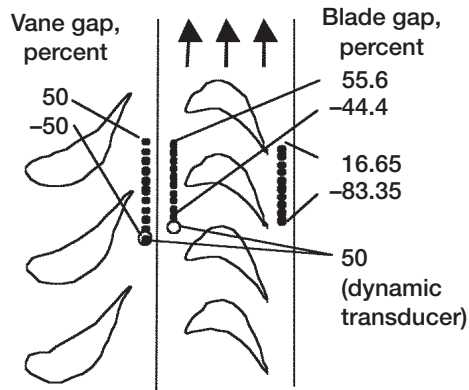


Figure 18.—Computational grid in disk cavity of high-pressure rig. (Athavale et al., 2001.)

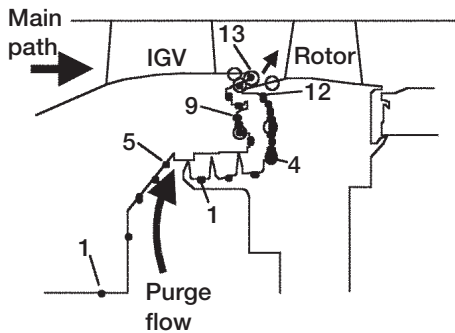


Figure 17.—Locations of pressure taps in United Technologies Research Corp. experimental rig. Dots denote steady-pressure, circle-transient pressure measurements. (Athavale et al., 2001.)

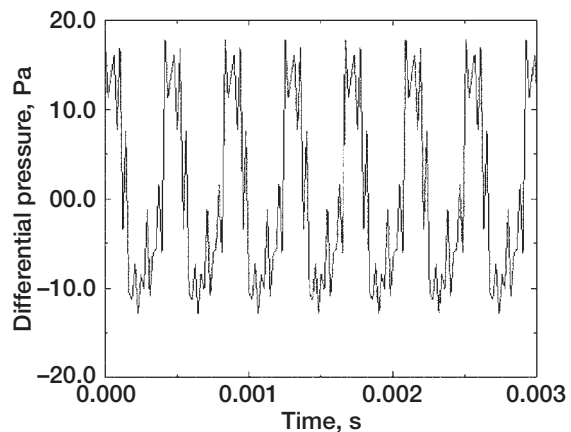


Figure 19.—Experimental transient trace for cavity pressure (with respect to a mean value) on rotor wall for 0 percent purge flow. (Athavale et al., 2001.)

Figure 19 shows the experimental pressure trace for 0 percent purge flow rate at the midcavity tap. Two points to be noted are (1) the amplitude of the experimental pressure trace is of the order of 12 Pa for a 0 percent purge flow rate (fig. 19), similar in magnitude to the simulated results, and (2) the calculated amplitude of pressure fluctuations increased with a higher (0.69 percent) purge flow rate (fig. 20).

Transient Pressures in Rim Seal

Experimental transient pressure at the pressure tap located under the stator vane platform has an amplitude of approximately 21 Pa for 0 percent cavity purge. This amplitude doubles to about 42 Pa at 2.83 percent purge flow rate. The calculated amplitude is approximately 50 Pa. These values are sensitive to the grid-clicking frequency.

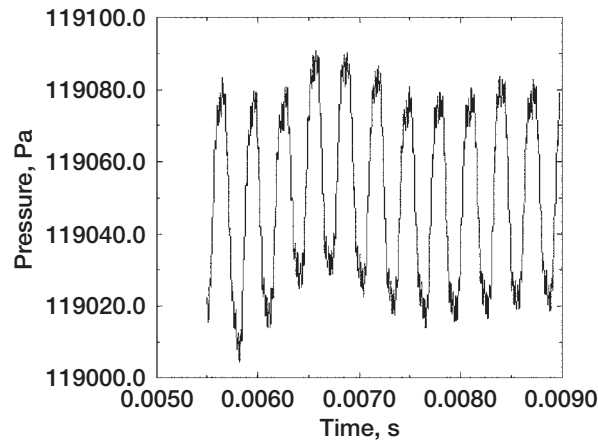


Figure 20.—Calculated transient trace for cavity pressure on rotor wall for 0.69 percent purge flow. (Athavale et al., 2001.)

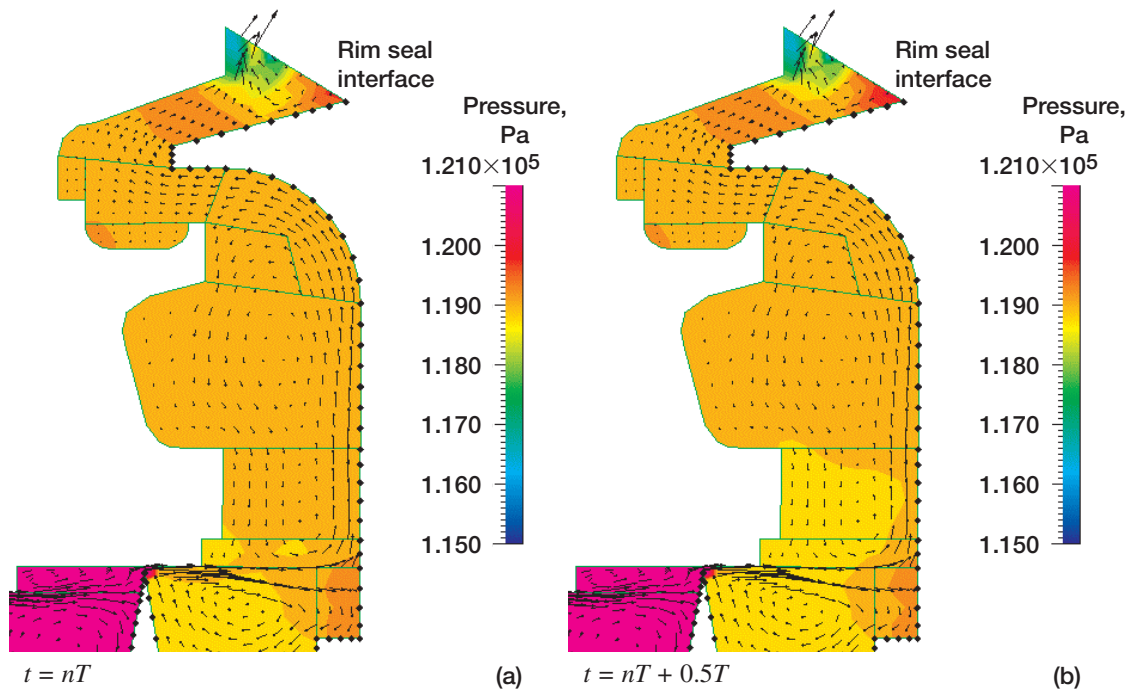


Figure 21.—Time-dependent cavity flows for 0.69 percent purge flow (absolute frame). (a) Time-transient pressures and (b) velocity vectors in cavity. $\eta = \text{Re}_{\text{feed}}/\text{Re}_{\text{turbine}}^{0.8} = 0.005$; t is time, n is cycle number, and T is cycle time. (Athavale et al., 2001.)

Figures 21 and 22 show the time-varying flow fields in the cavity for the two purge rates (0.69 and 2.83 percent; purge efficiency parameter $\eta = 0.005$ and 0.02 , respectively¹) at the aligned and midspan rotor positions. Figure 23 shows the surface pressure and velocity contours of the main path for a 2.83 percent purge flow rate. The cutting plane in these plots occupies a “midpassage” location in relation to the stator blade row. The recirculation zone in the rim seal present at the lower purge flow rate is absent at the higher purge flow rate. The recirculation allows some of the power stream

¹ $\eta = \frac{\text{Re}_{\text{feed}}}{\text{Re}_{\text{turbine}}^{0.8}} = \frac{(\dot{m}/2\pi r\mu)}{(\omega r^2/\nu)^{0.8}}$ where $\text{Re} = \text{Reynolds number}$, $r = \text{rotor rim radius}$, $\omega = \text{turbine angular rotation}$,

$\mu = \text{dynamic viscosity}$, $\nu = \text{kinematic viscosity}$, $\dot{m} = \text{purge gas mass flow rate}$.

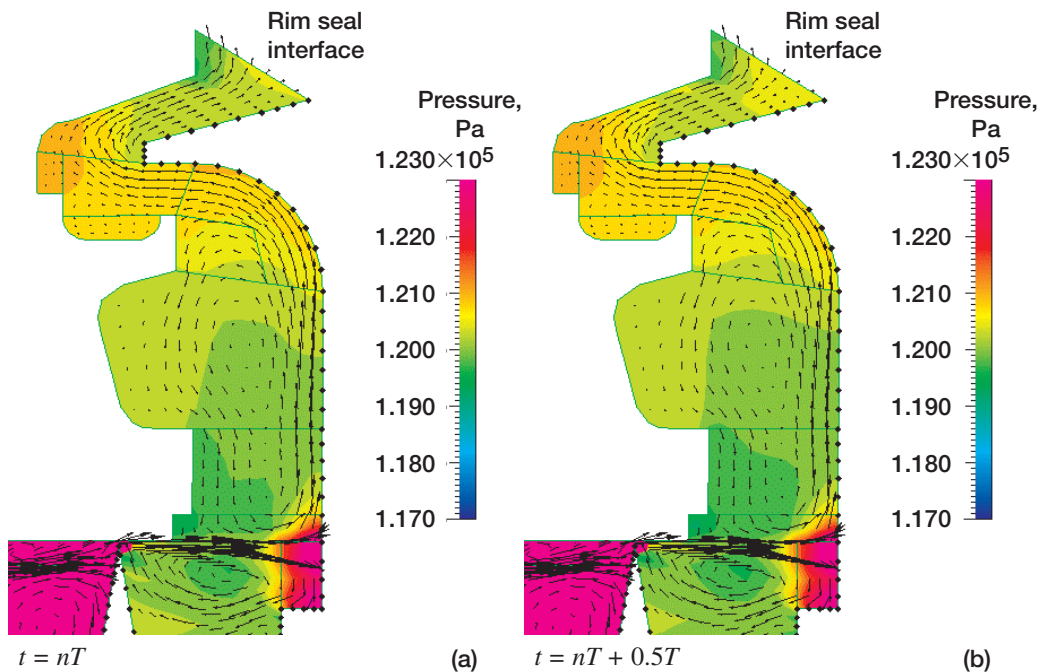


Figure 22.—Time-dependent cavity flows for 2.83 percent purge flow (absolute frame).
 (a) Time-transient pressure and (b) velocity vectors in cavity. $\eta = Re_{feed}/Re_{turbine}^{0.8} = 0.02$;
 t is time, n is cycle number, and T is cycle time. (Athavale et al., 2001.)

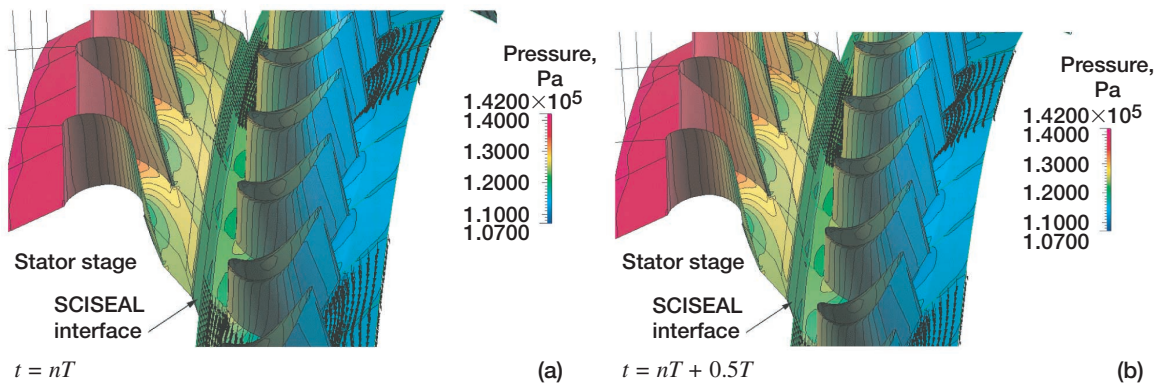


Figure 23.—Three-dimensional, time-dependent cavity flow (absolute frame). (a) Surface pressures and (b) hub velocity contours in main path at different times during passage of blade 2.83 percent purge. $\eta = Re_{feed}/Re_{turbine}^{0.8} = 0.02$; t is time, n is cycle number, and T is cycle time. (Athavale et al., 2001.)

to enter the rim seal area. This gas can then travel inside the cavity by both diffusion and convection. The higher purge rate precludes the entry of power stream even in the rim seal, and results in the observed noningestion. Two observations: (1) The interface velocities (flow coming from SCISEAL) show a tangential component that is lower than the rotor speed. This slow fluid alters the angle of attack near the roots of the rotor blades. (2) The rotor blades have the expected upstream pressure rise, which affects the flow in the rim seal and the cavity, although this disturbance is rather small.

Smout et al. (2002) in a CFD analysis of rim sealing cite some collaborative efforts involved in investigating rotating cavity ventilation, bearing cavity purge and cooling, pressure balance, and sealing rotor/stator gaps. A CFD analysis showed a step change in flow effectiveness or sealing

efficiency due to a shift to a higher frequency and lower amplitude fluctuation of the interface pressure. The analysis requires further study. The rotating cavity flow study found cyclonic and anticyclonic flows bifurcated at the outer radius. The cavity heat transfer was buoyancy dependent for Rossby² numbers less than approximately 3.5 (see Tam et al. method in part 2). Cavity heating influences the disk temperature, which in turn limits disk life. The turbine slinger determines the preswirl of cooling air entering the high-pressure turbine blades, and their work shows an optimum in hole discharge with negative preswirl from -0.25ω to -0.4ω as more effective. Also under investigation are the influence of heating in the compressor's stator-rotor well and compressor drive-cone cavity flows.

Cavity sealing is complex and has a significant effect on component and engine performance. However, several numerical tools help guide the designer and experimenter. In time, data, both from rig experiments and field results, will emerge to validate these efforts.

Blade Tip Sealing Flows

As demonstrated in part 1 for the YT-700 engine, changes in sealing affect the entire engine. It is important to evaluate how sealing and secondary flows at the blade tip and root alter stage flows and to understand how these disturbances propagate downstream. Doing so often necessitates simple sealing models. And lest the point get lost, the simplified models used to predict the rotordynamic forces due to imbalances in tip seal flow indeed seem to work, but they neglect the reality of the time-dependent character of that interface (see part 2, the models of Thomas, 1958; Alford, 1963; and Motoi et al., 2003). However, in defense of the rotordynamics work, CFD modeling of power-stream component problems, such as those of the compressor, combustor, and turbine, usually neglect the rotating flow imbalance characteristics of machines operating with eccentric loads and runout orbits. Song and Cho (2000) offer an inviscid, incompressible CFD analysis of nonuniform asymmetric compressor flow. It will be necessary to incorporate dynamics if greater understanding and finer percentages in efficiency are required.

For example, cavity and platform sealing flows must be combined with passage flows along with tip sealing and secondary flows. Figure 24 illustrates unshrouded compressor (and fan) and turbine average, or local, "snapshots" of tip flows. Similar illustrations are found in the text by Lakshminarayana (1996), and some sealing requirements are discussed in the sections Shroud Sealing and Abradables Standards and Blade Tip Sealing in part 1.

Compressor.—In the unshrouded compressor the axial leakage opposes the power-stream flow path, and the circumferential leakage across the blade tip opposes the rotation (figs. 24 and 25). These factors can lead to inversions in the velocity profiles and engender unstable vortex flow fields and fluctuations that are more intense at the pressure side of the blade tip. A significant flow loss can occur with large clearances, and blockage leads to local and eventual full stall. Compressor stall with the potential for unstart (engine unstart) is a major concern. Compressor rotor blades are usually quite thin with airfoil chord less at the tip than at the root and significant contouring from root to tip. In addition to the unstable flows the blade-to-tip clearance and blade passing space give rise to sonic oscillations and blade flutter.

Although compressor blades are contoured and slender, the ratio of blade thickness to tip clearance is large (e.g., factor of 10). The resulting L/D -equivalent circumferential channel flow depends on several factors. For example, in terms of case coordinates there will be regions of flow reversal, conceptualized in figure 25, that are dependent on blade geometry, edge sharpness,

² $Ro = V/2\omega L \sin \theta$, where V = fluid velocity, ω = angular rotation, L = scale length, and θ = angle between rotation axis and fluid motion.

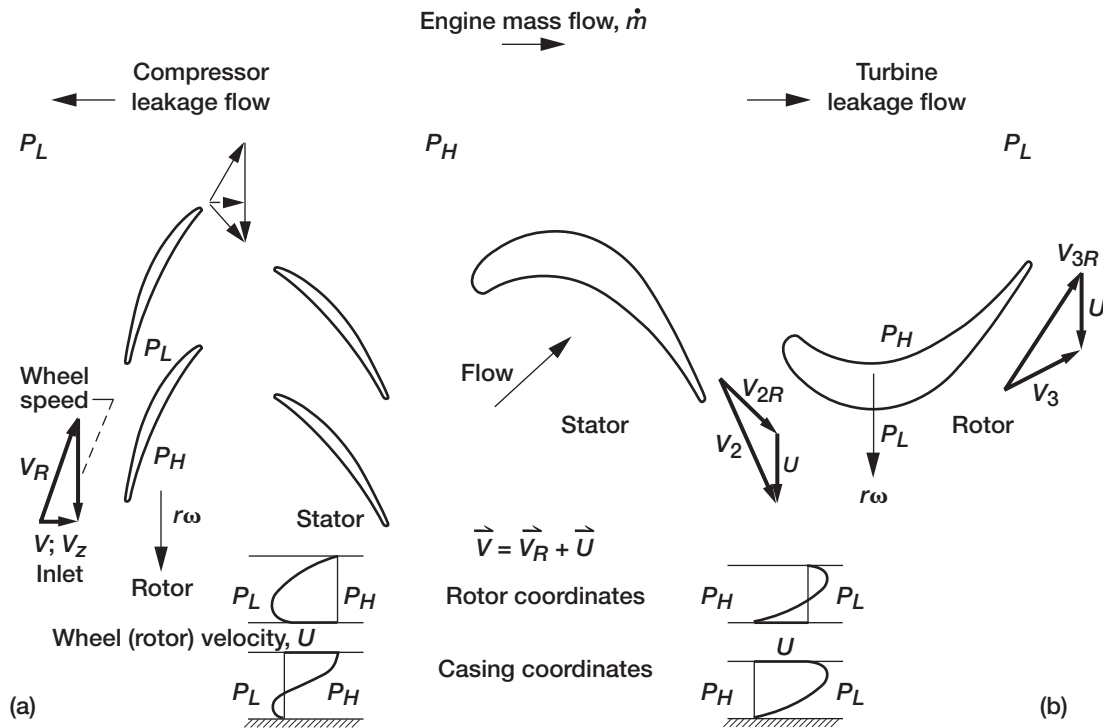


Figure 24.—Axial compressor (or fan) and turbine blade flow fields (absolute frame with velocity profiles for both absolute (casing) and relative (rotor) reference frames). (a) Compressor or fan rotor-stator blading. (b) Turbine rotor-stator blading. Symbols are defined in appendix.

clearance, casing wall treatment (e.g., smooth, felt metal, or honeycomb), pressure, and velocity as well as the compressor operating conditions. At very small clearances (e.g., <1 percent of tip chord) the reversal region is small and close to the shroud, casing, or wall. At large clearances (e.g., 4 to 5 percent of tip chord), the reversal region expands away from the shroud, casing, or wall. In rotor coordinates these reversals are not noted. In addition, the total pressure gradient opposes the axial mass flow. Normal-operation tip gap is in the range 1 to 2 percent of tip chord, depending on engine size.

These conditions lead to primary leakage within the passage inlet or leading-edge (LE) region, with vortex shedding extending across to the suction surface near the trailing edge (TE) of the adjacent, on-coming blade. Near stall, however, this vortex remains at partial chord and extends over the adjacent blade, altering the angle of attack. At the blade trailing edge the Kutta condition vortex forms, and the pressure gradient coupled with the sharp trailing edge forces an axial flow inward along the blade surface. At the leading edge the flow is forced out and around the stagnation region, couples with the primary leakage zone, and extends across the passage toward its low-pressure side and opposing the rotational velocity. These conditions are seen with tip clearance flows in the transonic compressor rotors as reported by Van Zante et al. (1999) and illustrated in figures 26 to 28. Usually, in transonic compressors by the time the flow reaches nearly the third or fourth stage, it is subsonic.

Copenhaver et al. (1996) investigated four tip clearance gaps at 0.0, 0.27, 1.0, and 1.87 percent of the ratio of tip clearance to tip chord. The reported rotor efficiency dropped 6 points when clearance ratio was increased from 0.27 to 1.87 percent, flow decreased 30 percent, and there was a stronger interaction between the tip leakage and the flow passage shock. In a prior investigation of a fan at ratios of tip clearance to tip chord of 0.27, 0.75, and 1.25 percent, Adamczyk et al. (1993) found that flow and peak pressure rise increased when clearance was decreased and was more stable with lower clearance at the leading edge. As illustrated in figures 26 to 28 the leakage region was most

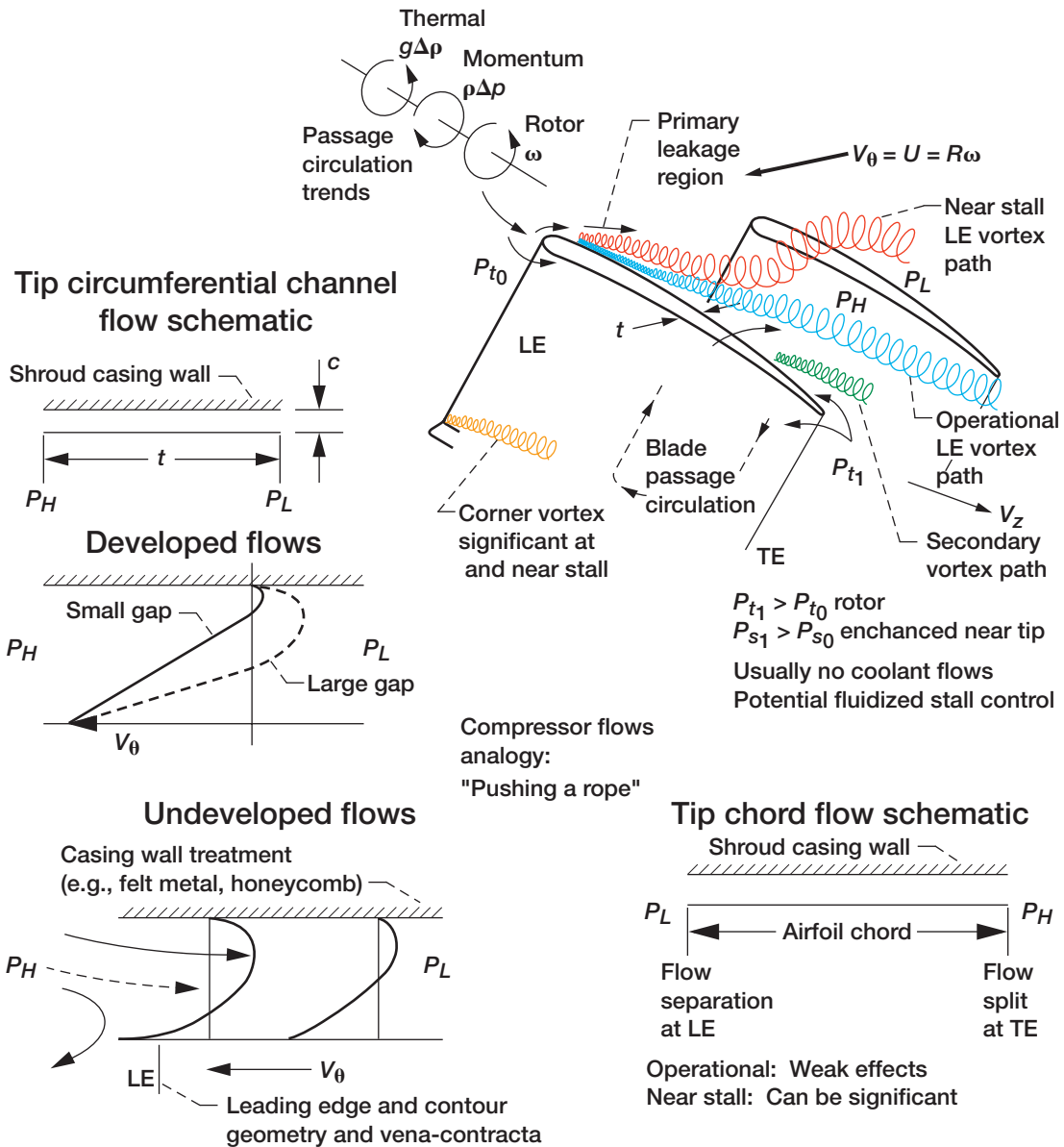


Figure 25.—Average tip sealing flows for conceptual unshrouded compressor (absolute frame). Symbols are defined in appendix.

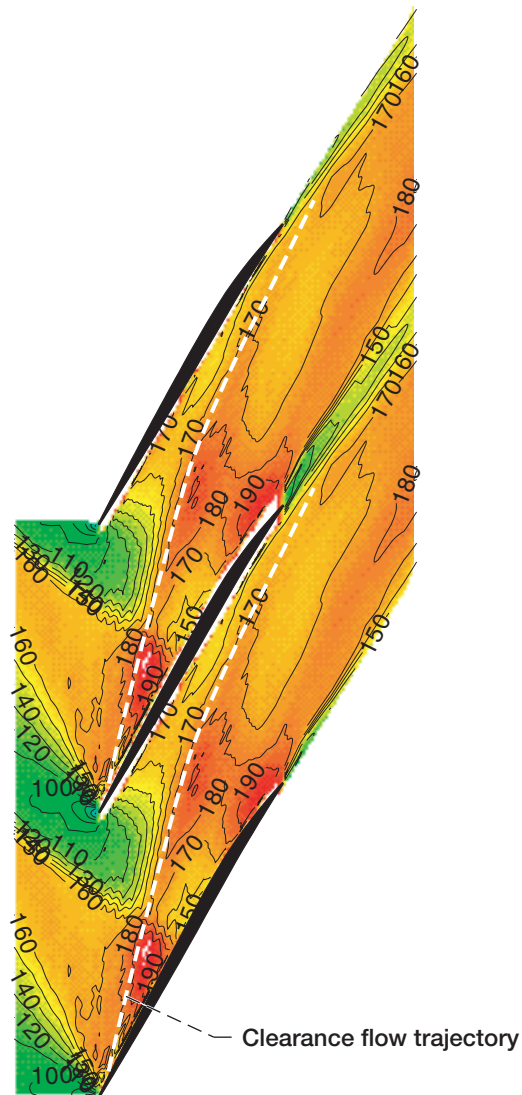


Figure 26.—Contours of axial velocity (m/s) on 92-percent-span stream surface from LDV measurements (no frame dependence). (Van Zante et al., 1999.)

pronounced near the leading edge with the effects carried into adjacent blades and into downstream stages. Also, note that this configuration is convergent with respect to the axial pressure gradient, a known factor used in sealing technology to enhance stability. Although these figures illustrate complex flow patterns, they represent only an “average snapshot” of the time-dependent flow field. This average representation reoccurs at the blade passing frequency and is additionally complicated by mismatched rotor and stator blading. Under these conditions case ovalization and offset rotor will tend to drive instabilities. See part 2 and prior discussion on case clearance control.

Fan.—Fan blade tip and root seals have leakage flows that oppose the main-stream flow direction and tip flows that oppose rotation, and in this respect the flows are similar to those in the compressor. The inlet axial passage is highly convergent with large contoured swept blades extending to the shroud seals (see part 1). The hub curvature and centrifugal forces serve to mitigate foreign object damage (dirt, sand, and other materials ingested into the compressor). Using hub and core bleed rather than casing air bleed enhances bearing life because the buffer gas in the bearing

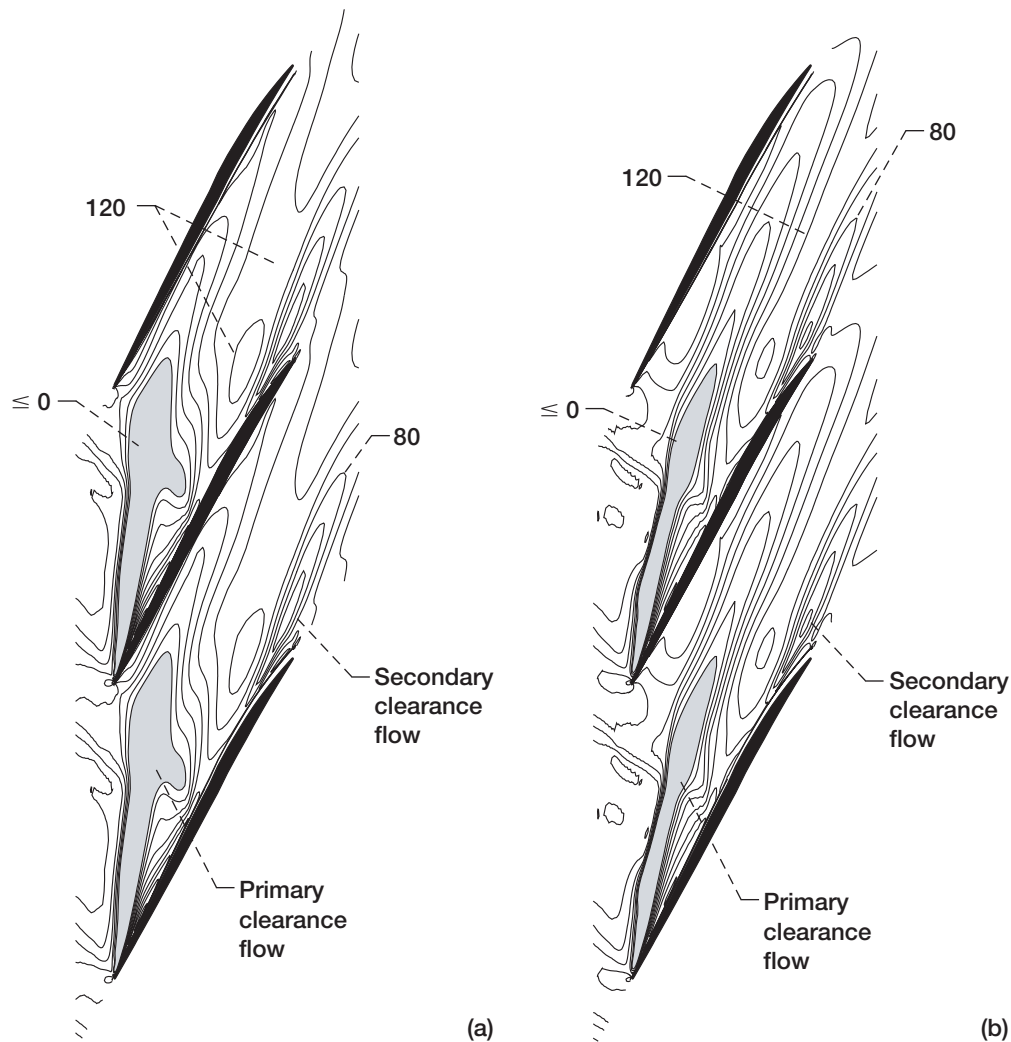


Figure 27.—Axial velocity contours (starting at 0 m/s with 20-m/s intervals) at blade tip grid plane for radial grid spacing in clearance gap of configurations 1 and 3, near peak efficiency (same in either relative or absolute frame). (a) Configuration 1 (constant cell size). (b) Configuration 3 (cells clustered near shroud). (Van Zante et al., 1999.)

compartment is cleaner. In commercial engines transonic speeds within the cowl are to be avoided because shocks engender complex flows and losses. For example, the NASA Energy Efficient Engine (E³) flight Mach number is 0.8 at 10.67 km (35 000 ft), but the fan is transonic with a fan tip speed of 411.5 m/s (1350 ft/s) (Davis and Stearns, 1985). These values imply subsonic flows at the hub with transonic circumferential velocity within the blade passage and supersonic to no-slip velocities in the tip sealing gap. At the tip, if the rotating flow within the gap were two dimensional and axisymmetric (coaxial cylinders) with one wall in motion (or counterrotation), sharp changes in the shear flows would occur but no shocks. However, for the bladed configuration (fan or compressor) shocks appear at the leading edge and at the pressure surface and extend in a radial direction and toward the case, similar to a standing shock on top of an airplane wing. The shock strength diminishes radially toward the case and axially along the blade chord with the possibility of expansion fans at the trailing edge.

Even though the wheel tip speeds are transonic, which implies that the relative velocity at the blade leading edge is also transonic, at the trailing edge the relative velocity is high subsonic (fig. 29).

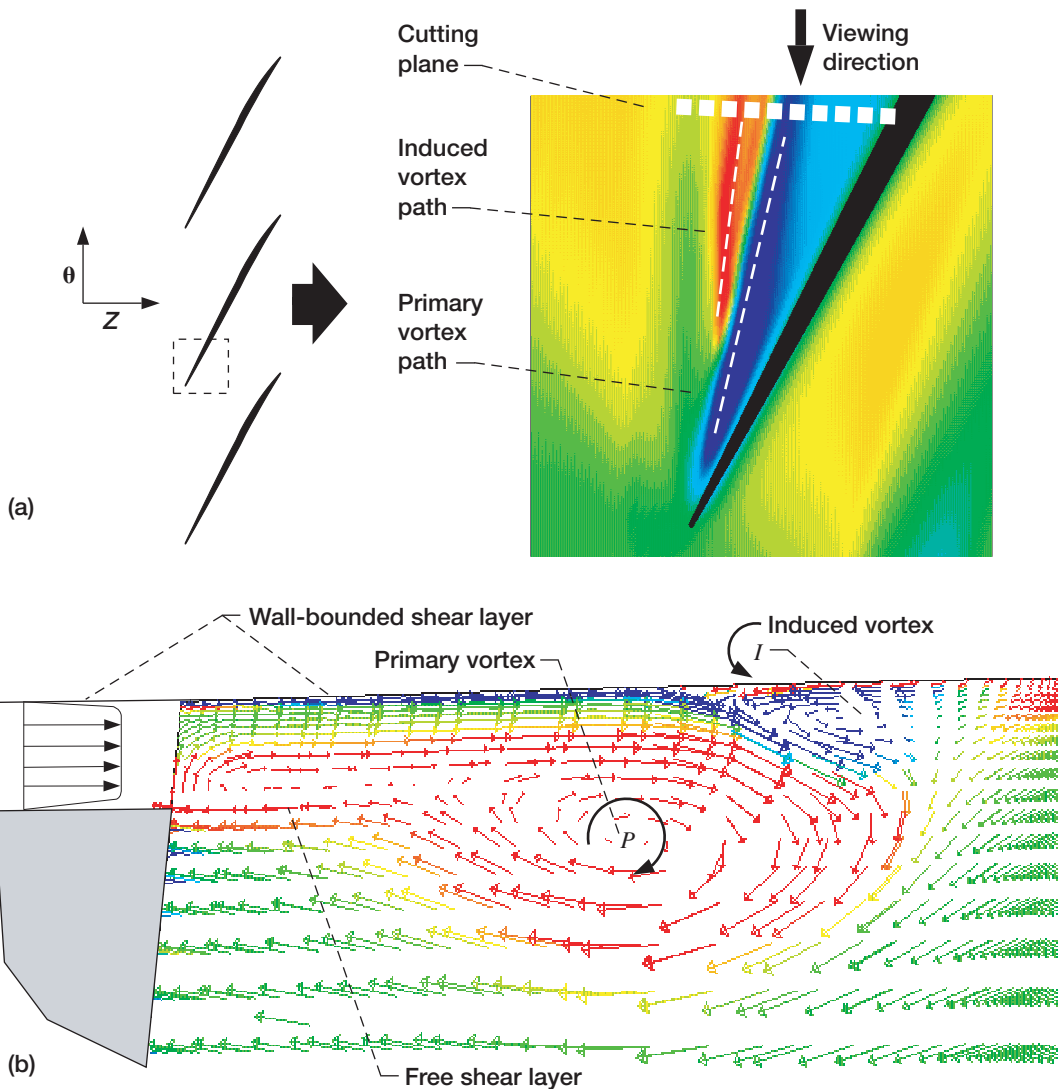


Figure 28.—Visualization of primary and induced clearance vortices. (a) Axial velocity at 6 percent of clearance gap height from shroud. (b) Projection of relative velocity vectors on $Z-r$ cutting plane as viewed in positive θ direction colored by θ -component of velocity. Suction surface at right edge of figure. Note that the velocity profile, upper left of figure, is valid only for cascades. Symbols are defined in appendix. (Van Zante et al., 1999.)

Strazisar et al. (1985, 1989), using laser anemometry, surveyed the flow passages of a transonic fan, providing blade-to-blade and streamwise distribution of the relative Mach number (figs. 30 and 31, respectively). A shock develops within the flow passage and provides most of the pressure rise with some diffusion through the passage flow (fig. 32). The shock is, in reality, a region not a distinct locus, and its location and strength depend on the backpressure (fig. 33) and time unsteadiness of the flow field. For supersonic flow a shock similar to a bow shock extends across the passage near the leading edge (fig. 29); the location can range from the trailing edge to nearly the leading edge, engendering unstart (not a good thing to any pilot or passenger).

Bilwakesh and Koch (1972) studied a 0.5-hub/tip-radius-ratio compressor stage up to 457 m/s (1500 ft/s) tip speed with variable chamber inlet guide vanes (IGV) and a variable-stagger stator. At design speeds the data were within 1 percent of design, which was not specified in their paper. Analytical results on the rotor tip shock structure, the deviation angle, and the part-span shroud losses at different operating conditions show that variable-geometry blading gave efficient operation at

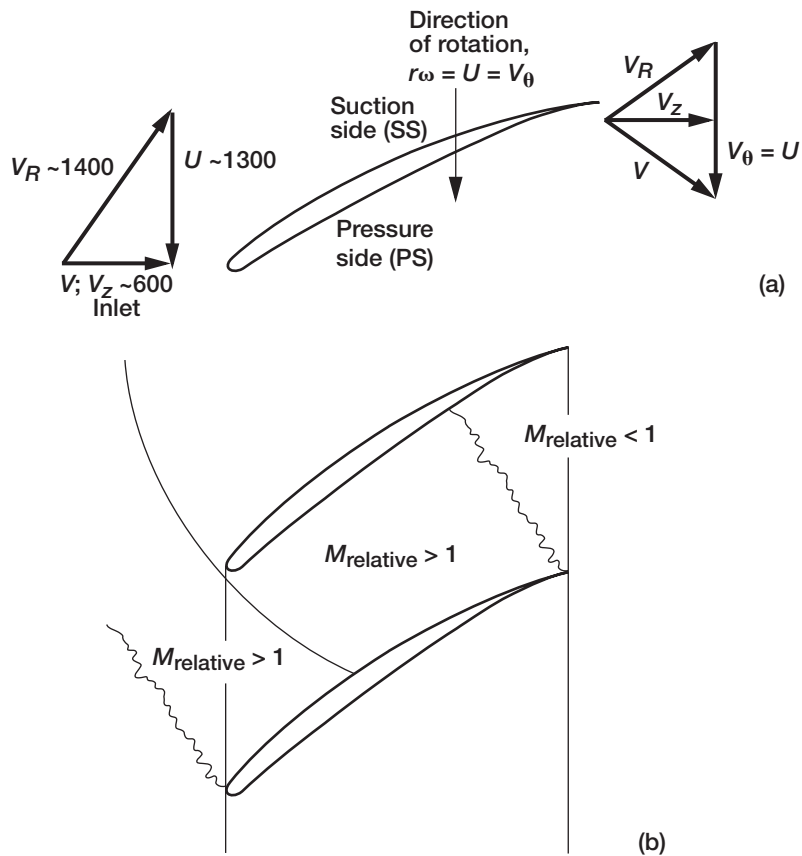


Figure 29.—Compressor blade passage inlet flow characterization (after Strazisar, private communication). (a) Conceptual blade characteristics (absolute frame). (b) Supersonic flow field (relative frame). Symbols are defined in appendix.

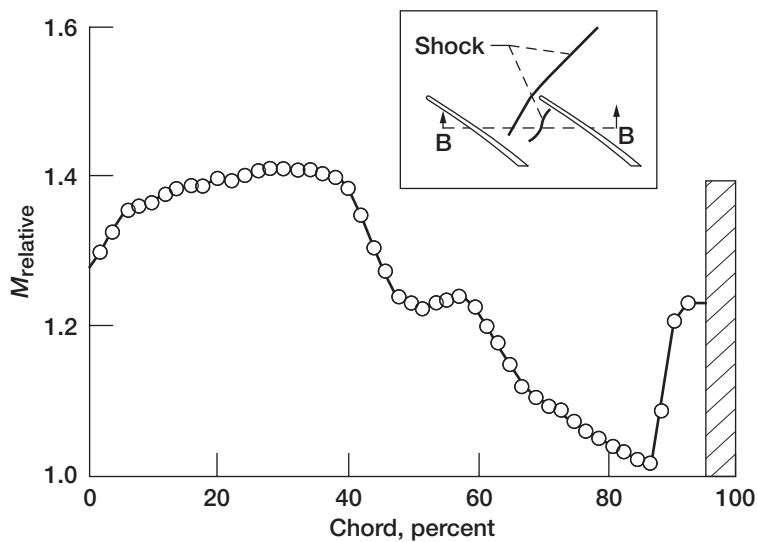


Figure 30.—Blade-to-blade distribution (view B-B) of relative Mach number at 30 percent span and 30 percent chord at peak efficiency. (Strazisar, 1985.)

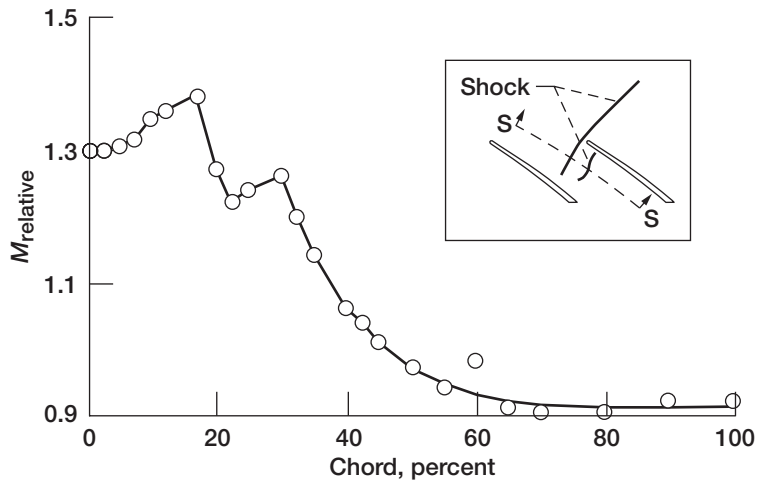


Figure 31.—Streamwise distribution (view S-S) of *relative* Mach number at 30 percent span and 60 percent blade pitch from suction surface at peak efficiency. (Strazisar, 1985.)

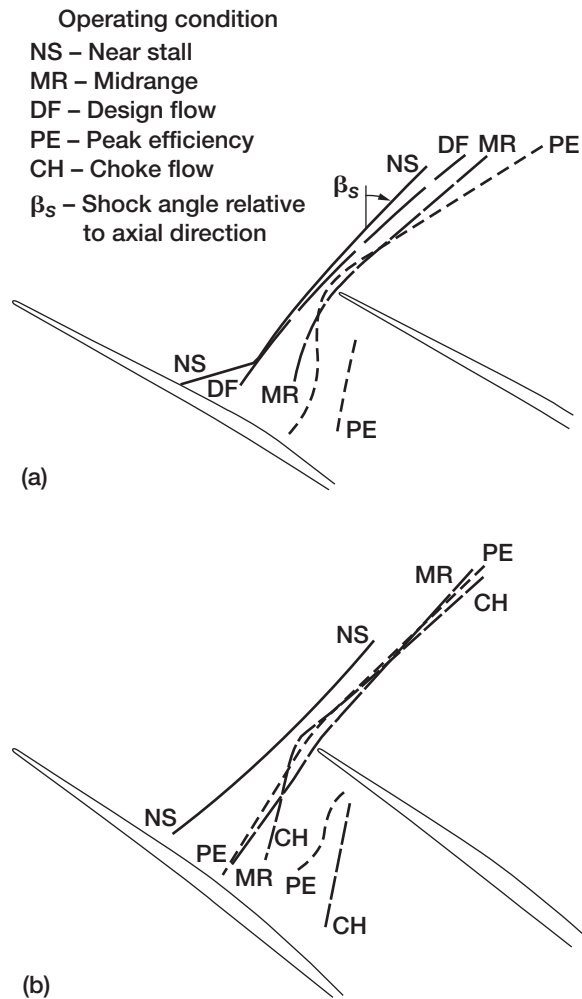


Figure 32.—Rotor shock structure at design speed for various operating conditions. (Strazisar, 1985.)
(a) 10 percent span. (b) 30 percent span.

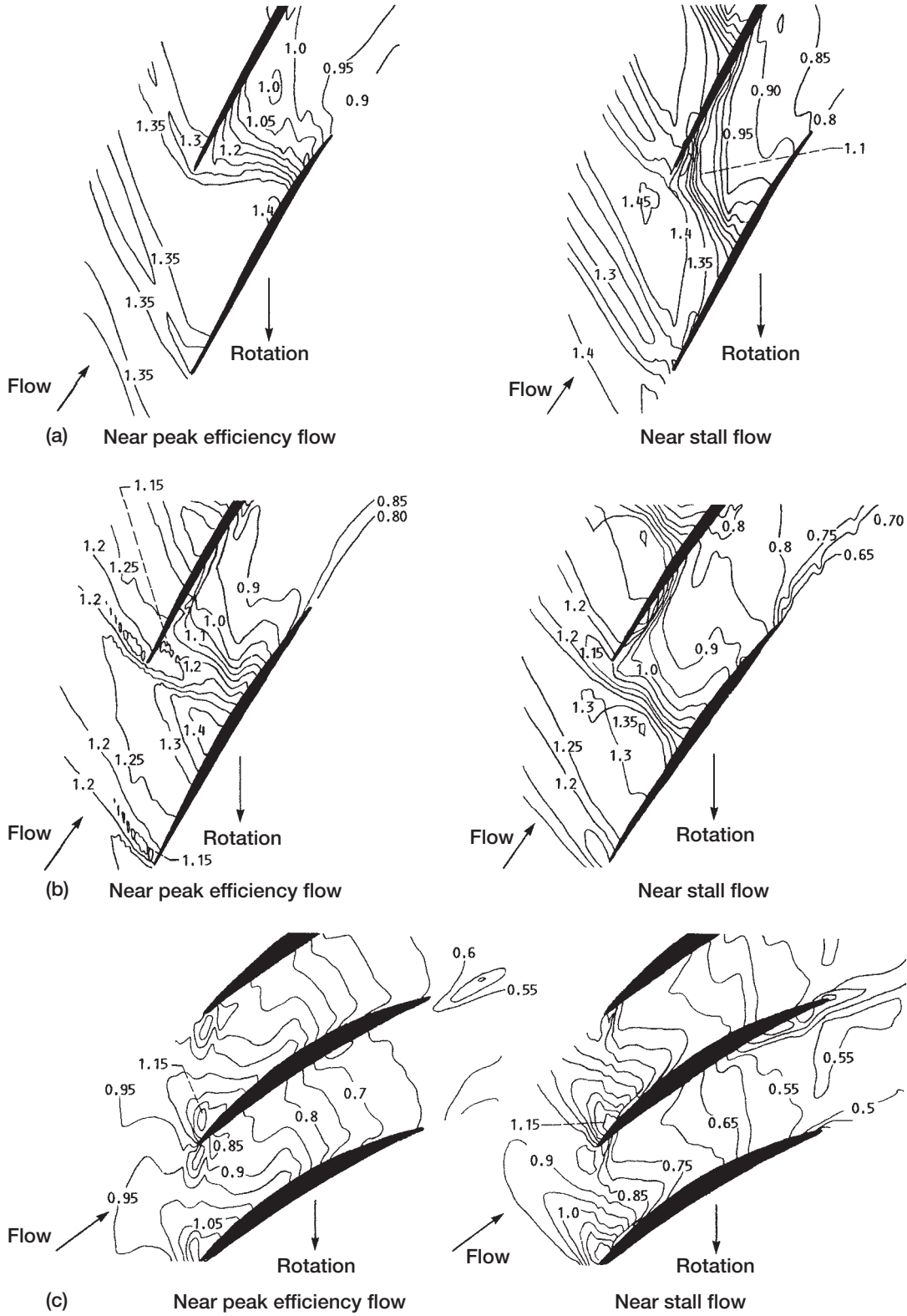


Figure 33.—Contour plots of *relative* Mach numbers at flow near peak efficiency and near stall (rotating frame). (a) 10 percent span from shroud. (b) 30 percent span from shroud. (c) 70 percent span from shroud. (Strazisar et al., 1989, fig. 17.)

adequate stall margin. Closing the IGV to 40° provided flexibility for operation at off-design conditions, although inlet flow distortions caused considerable losses at 0° IGV. The use of 40° IGV enabled partial stall recovery.

Fan blade (or compressor) shroud sealing is highly dependent on the relative Mach number of the flow field. The type of shroud seal varies and can be a multiple-ribbed polymer composite, similar to labyrinth sealing with circumferential flow blocks, to rather a plain cylindrical interface with acoustical treatment (see part 1). For each of these sealing methods, fan tip acoustics are critical and require further study. At the platform leakage is also periodic, with blade passing and midspan reingestion into the main stream causing passage disturbances that propagate into the compressor. Platform sealing is usually of the labyrinth type.

Turbine.—In the unshrouded turbine similarities to compressor tip flows persist. The turbine tip flow field engenders vortex flows that give rise to flow blockage with subsequent decreases in efficiency. Coolant air is routed from the compressor through the disk cavity and disk rim into passages within the turbine blades that provide film cooling and, along with the thermal barrier coating, thermally protect the blade. These coolant flows couple with the pressure-side-to-suction-side passage vortex and present passage blockage that decreases through mass flows and turbine work. However, without coolant flows the turbomachine will not last very long.

Turbine blades are usually highly contoured, thick, and well cooled compared to the compressor blades, which are thin and uncooled. In casing coordinates the circumferential and axial pressure gradients are in the direction of rotation and flow, respectively (opposite those of the compressor or fan). Although flow instabilities are present, the turbine will operate effectively over a large range of perturbed flows and at off-design conditions. Even blades that appeared “chewed” at the tips (e.g., due to rubbing) seem to provide reasonable performance, although this is not the case for the compressor. The major vortex patterns, conceptualized in figure 34, form on the low-pressure surface and at the abrupt curvature change on the pressure surface. The stronger low-pressure-side (suction side) vortex is usually tight with respect to the blade because leakage and rotation are in the same direction. All these leakages are complicated by the coolant flows at the tip, at the leading and trailing edges, and on the surface and platform. The major surface film cooling is on the pressure side and in the platform regions, with a few cooling and separation control holes on the suction side. The tip flows can contribute heavily to the leakage flows and blade tip casing heat transfer.

For example, Ameri et al. (1999, 2000) found that the thermal loading of all surfaces increased with increased turbine tip clearance but dropped with introduction of a back-step recess, with a marked drop at the blade tip but little effect on casing heat transfer.

Two-dimensional and linear cascade flows are useful in documenting average passage information, but they fail to invoke the reality of time-unsteady flows due to rotating blade/vane interactions. Equivalent computational cascade codes provide insights but, again, are lacking rotational effects and the physics of the actual flows within the stages as discussed in part 2 and shown in equation (A4), repeated below.

$$\frac{\partial(\rho \tilde{U} J)}{\partial t} + \nabla \cdot (\rho J \tilde{U} \tilde{U}) = -J \nabla p - J \left[\underbrace{\rho \bar{\omega}_p \times (\bar{\omega}_p \times \bar{r})}_{\text{Centrifugal}} + \underbrace{2\rho \bar{\omega}_p \times \tilde{U}}_{\text{Coriolis}} \right] + \underbrace{J \nabla \tilde{\tau}}_{\text{Body force}} + J \rho \bar{g}$$

Centrifugal
Shear

↓
↓

These “snapshots” of the flow field can be deceptive. For example in a transonic rotor-stator configuration, shocks appear and vanish all within the same blade passage sequence. Also, it is known that by the third stage of a multistage compressor most of the flows are subsonic (e.g., from shock

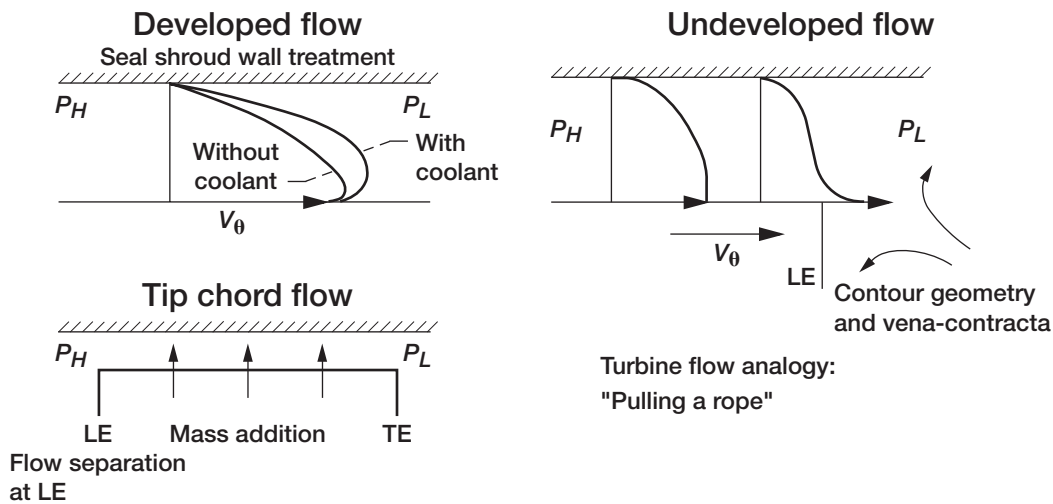
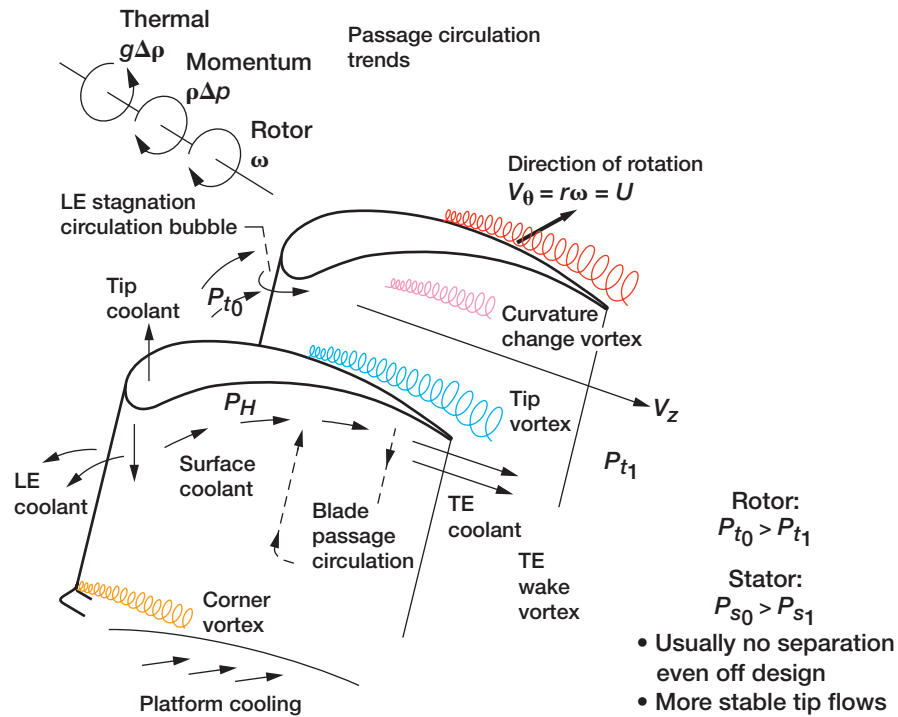


Figure 34.—Average flows for conceptual unshrouded turbine tip sealing (absolute frame). Symbols are defined in appendix.

smearing and temperature rise). These snapshot vortical structures pass on through the fan and compressor into the combustor. Even though diffused, vortical structures can affect the combustion, providing hot spots into the turbine and local high-velocity zones with potential screech within the exhaust cone that must be suppressed.

In more advanced engines, these time-unsteady effects and controlled shocks become the basis of the system. Two examples are the pulse detonation engine (PDE) and the wave rotor topping cycle (e.g., Wilson et al., 1997; see PDE in reference list). Adding fuel in the transonic fan duct or in later compressor stages would give yet another type of augmented cycle. Although jet and rocket engines are conceptually simple systems, in reality the physics are quite complex. Nevertheless, these aerospace engines work well.

As interesting as tip flows are, the details are difficult to capture and most design codes minimize computations within the tip clearance region, replacing them with simple models. It becomes costly to include the details necessary to capture complex tip flow fields in a fan, compressor, or turbine stage. However, in such details are challenges that provide opportunities for engine performance improvements. As a result most experiments are run to support validation and implementation of design codes (see part 1). We now look at components attached to the engine case without which the engine would not function.

Engine Externals

Without engine externals, no smoke, no fire, no thrust—in short, no good. Mike Miller (Boeing “Chief Trouble Shooter,” now retired) presented in some detail the case for engine externals. Miller et al. (1998) writes that “between the engine case and the nacelle cowling there exists a complex space overflowing with pipes, wires, components and challenges (fig. 35). This is the world of engine externals, a cramped, noisy, hot, high vibration world where the engine controls and engine powered services are located. Engine externals are seldom discussed, researched or understood by the aerospace community. This is the realm of the maintenance engineer, airline mechanic and the systems design engineer.” For one airline the combined estimate of inflight shutdowns amounted to about 40 percent of their unscheduled maintenance, 80 percent of which related to engine externals (fig. 36). Engine externals account for nearly one-third of the maintenance budget. A look at the Boeing 777 fan duct leakage area of 4387 mm² (6.8 in.²) per nacelle translates into an operating-empty weight penalty of 9074 N (2040 lb) and a thrust specific fuel consumption increase of 0.38 percent. If there were no seals, the penalties would become prohibitive and a 445-N (100-lb) seal weight is quite acceptable.

Leakage areas in older aircraft range to 0.4 percent of fan duct nozzle area with current targets at an aggressive 0.1 percent (table I). Figure 37 shows that a typical Boeing 777 fan duct seal for one nacelle is nearly 24.7 m (81 ft) long. Miller cites opportunities in good seal designs as well as in cooling analysis, fire extinguishing, cowl vent designs, and high-temperature (370 °C; 700 °F)

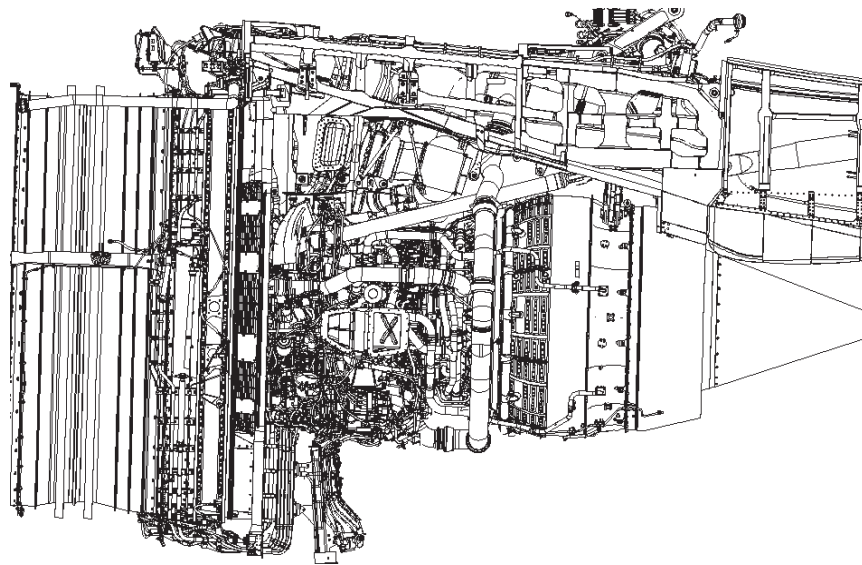


Figure 35.—Typical Boeing 777 engine with strut and externals installed.
(Miller et al., 1998.) Courtesy The Boeing Company.

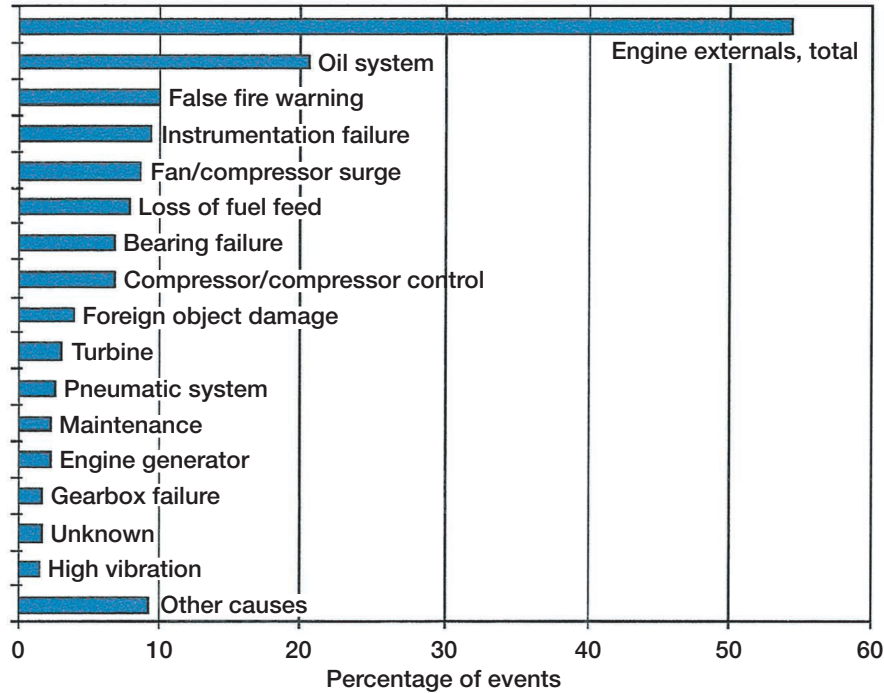


Figure 36.—Inflight shutdowns of Boeing twin-engine airplane fleet, 1980 and after. (Miller et al., 1998). Courtesy The Boeing Company.

TABLE I.—LEAKAGE GOALS FOR NACELLES (TYPICAL)
[Miller, et al., 1998. Courtesy The Boeing Company.]

Airplane	Nominal fan nozzle area		Target leakage area	
	cm ²	in. ²	in. ²	Percent of nozzle area
737-300/400/500	7 484	1 160	4.64	0.40
757-200	13 826	2 143	3.2	0.15
767-200/300	17 955	2 783	4.2	0.15
777-200/300	29 245	4 533	6.8	0.15
737-600/700/800	7 742	1 200	1.2	0.10

wiring. Inappropriate cowl venting can create shocks or flow separation that severely degrades performance. Fire suppression location and type with ability to positively extinguish is not fully known. High-temperature wiring is a requirement for next-generation engines.

One enormous, but very practical, set of pipes wrapped about the aft part of the engine with a scoop penetrating the fan duct is for active clearance control (ACC). (See figs. 35 and 41.) A split-scoop in the fan duct recovers relatively inexpensive air and meters and distributes that air through pipes wrapped around the case. The cooling air impinges on the high-pressure turbine (HPT) case and on the low-pressure turbine (LPT) case at blade stages to control clearances between the blade tips and the shroud seals attached to the case (fig. 38). These clearances are determined primarily from the flight profile and the engine speed and temperature. The cooling air is sufficient to close down the clearances to the point of rub, which is undesirable, and a positive clearance is maintained (fig. 39). Once determined, the clearance-time profile is programmed into and controlled by the engine full-authority digital electronic controller (FADEC). A firewall baffle is used to ensure that these hot gases do not circulate forward within the externals compartment. The system also permits case heating with compressor air during cold startup.

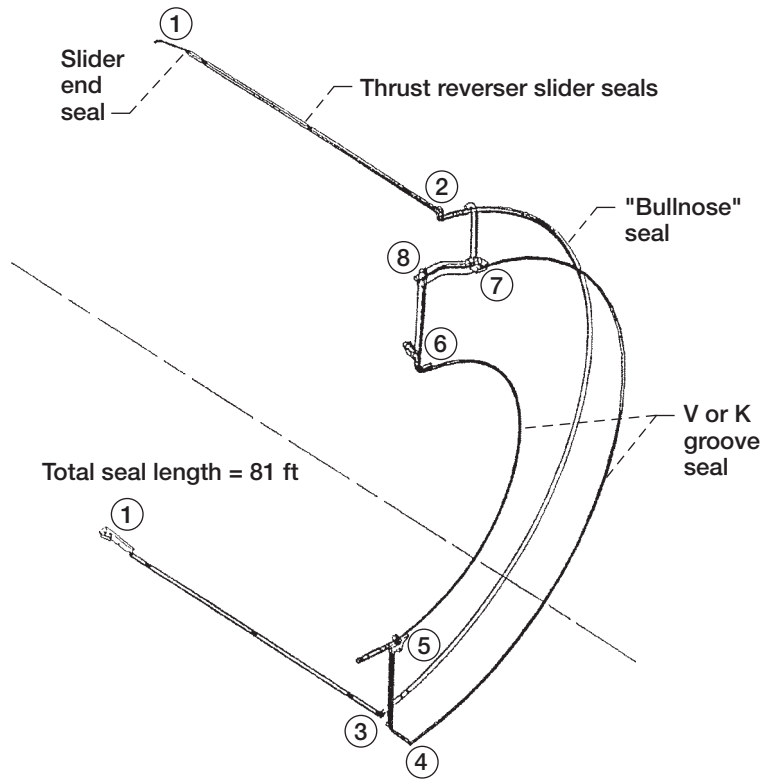


Figure 37.—Typical Boeing 777 fan duct seals. (Miller et al., 1998.)
 Courtesy The Boeing Company.

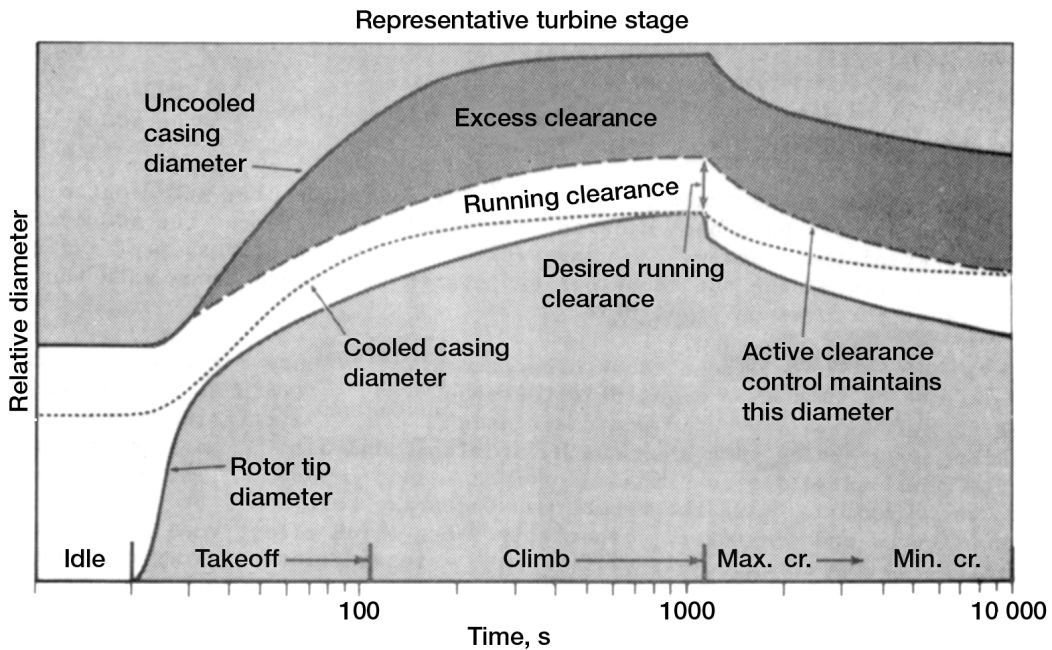


Figure 38.—HPT/LPT active clearance control system. (Halila et al., 1982, modified by fig. 43.)

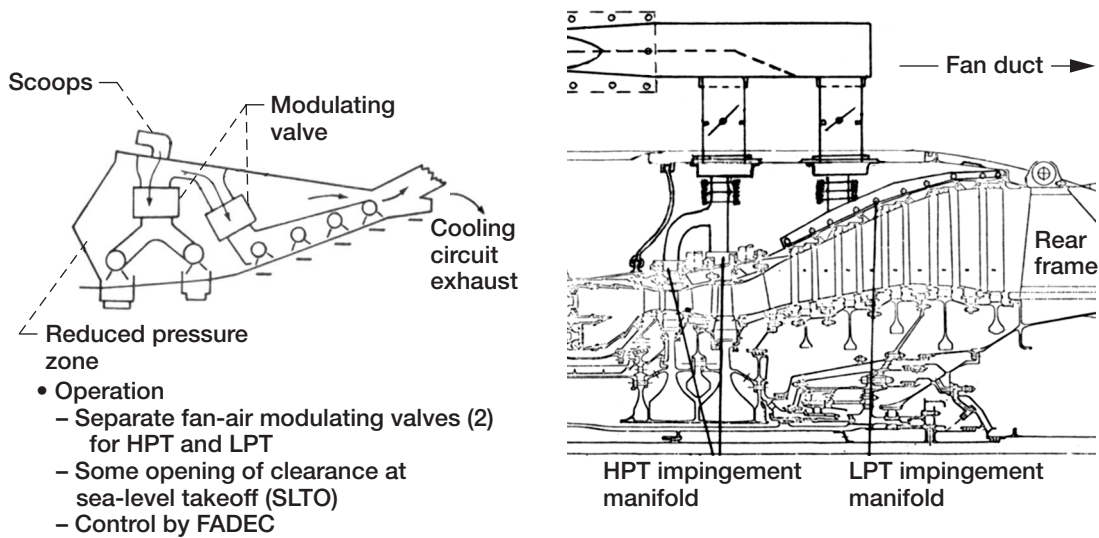


Figure 39.—Active clearance control operational profile. (Halila et al., 1982.)

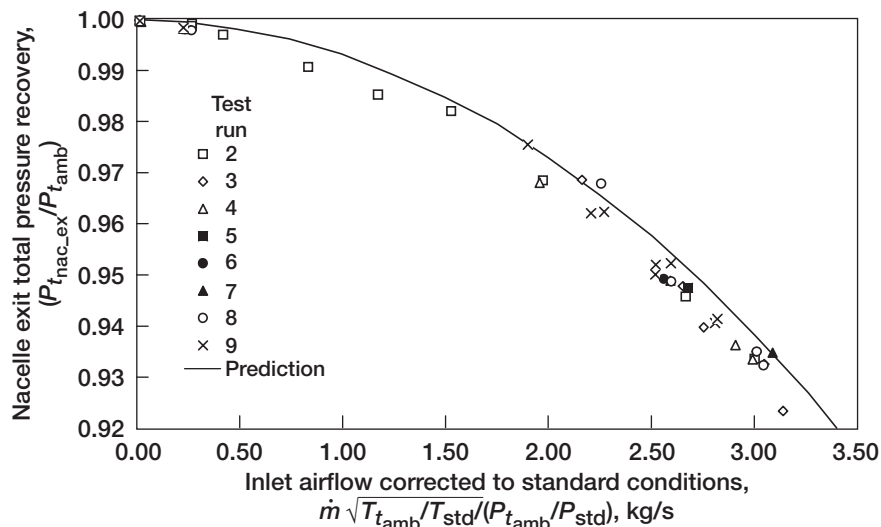


Figure 40.—Predictions compared with full-scale aircraft ground test data. (Ginn, 1998.) Courtesy Lockheed-Martin Company.

Ginn (1998) introduced an experimental effort to characterize engine external flow fields by using a 20-percent scale model of the engine nacelle, whereas Miller et al. (1998) employed a full-scale mockup model in seal testing. In Ginn's model all geometric features considered to have an effect on total pressure loss were considered. The corrected reduced mass flow as a function of station total pressure recovery fraction agreed well with predictions and with full-scale aircraft ground test data (fig. 40).

Stoner (1998) defines engine externals: "Engine external components include all the fluid carrying, electron carrying, and support devices that are needed to operate the propulsion system," are housed between the engine case and the cowl, and interact with the EBU's or engine buildup components (e.g., inlet, fan cowl, thrust reverser, core cowl, and nozzle) as cited by Miller et al.

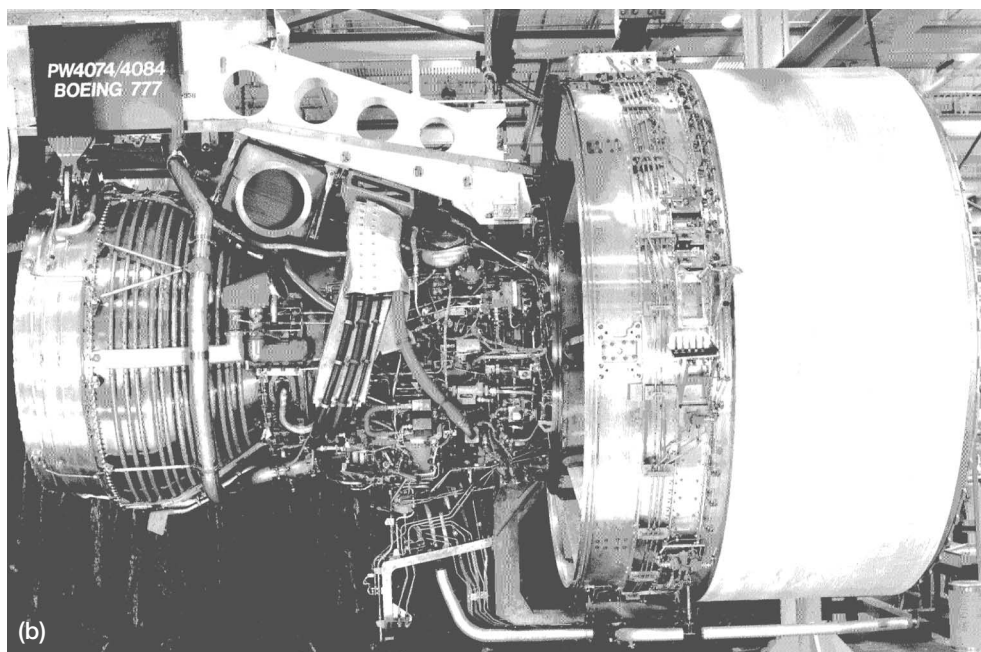
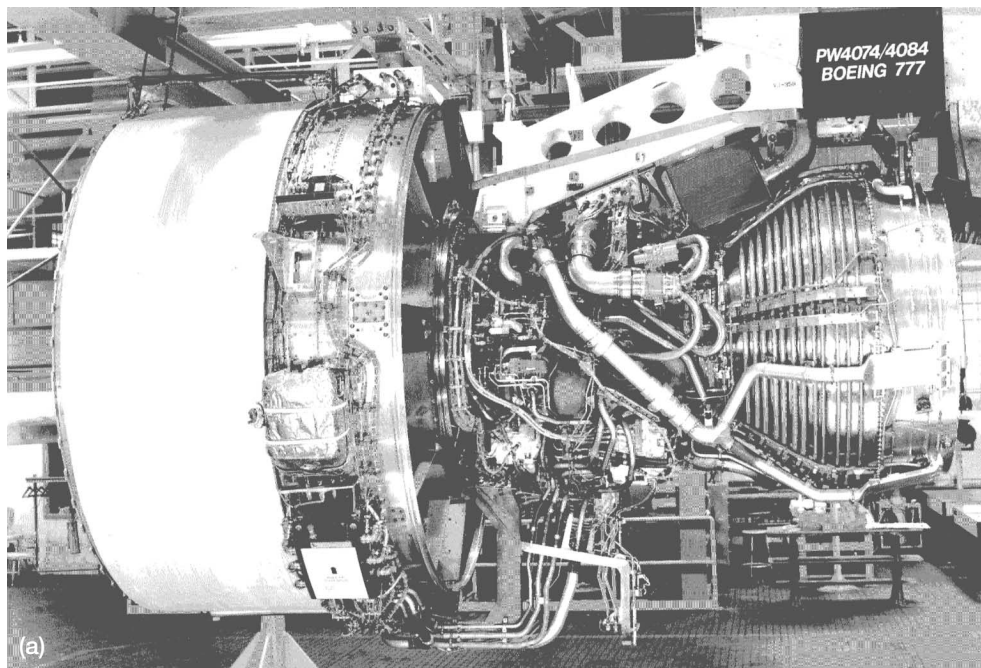


Figure 41.—Modern aeronautical gas turbine engine. (a) Left-hand side.
(b) Right-hand side. (Stoner, 1998.) Courtesy Pratt & Whitney.

(1998). There are a myriad of components (fig. 41): hundreds of tubes, maybe 400 hoses and 700 brackets, 100 control system components, and a few hundred more EBU and nacelle components, all secured by thousands of fasteners. There are pumps, heat exchangers, ducts, clamps, sensors, switches, generators, electrical harnesses, and many others without which the engine cannot function. The failure of any one of these components to perform its intended function requires a maintenance action, delay of a flight, or in-flight shutdown. The environment in which these components must function is closely tied to the basic design requirements and life and reliability. Consequently, the components' operating environment must be understood and controlled by careful design, testing, and field service feedback.

As shown in figures 41 and 42 a look under the cowl of a modern aeronautical gas turbine is bewildering. In addition to thrust the engine must produce the mechanical and electrical power required by the aircraft (the auxiliary power unit (APU) does unload and provide engine support). These engines are hot, vibrate, and function under adverse loadings. Customer requirements with two-engine aircraft (e.g., the Boeing 777) for extended operations of more than 1 hour from an adequate airport and over mostly open water are called extended-range, twin-engine operations ("engines turn or passengers swim", or ETOPS). At entry into service (EIS) ETOPS demands high component reliability, which requires redundancy and/or long life with high reliability, usually meaning less than one failure in 1000 components. Engine case temperatures run from ambient to over 650 °C (1200 °F) in the hot (gas generator) section (high-pressure compressor, combustor, high-pressure turbine). This heat is dissipated by conduction, convection, and radiation into the case cooling air derived from the fan. Environmental air and engine power influence the externals' operating temperatures (fig. 43). The flight cycle (fig. 44)—taxi, takeoff, climb, cruise, decent, thrust reversal, taxi, and soak-back—all place high thermomechanical demands on externals (fig. 45). Although the engine rotors are carefully balanced, case-transmitted vibrations are primarily due to rotor unbalance or perturbations. Other sources such as flow through ducting, tubes, inlets, pumps, valves, etc., all contribute to the stress cycling and vibration of externals.



Figure 42.—Engine on wing (Boeing 737–600). Courtesy The Boeing Company Commercial Aircraft Division.

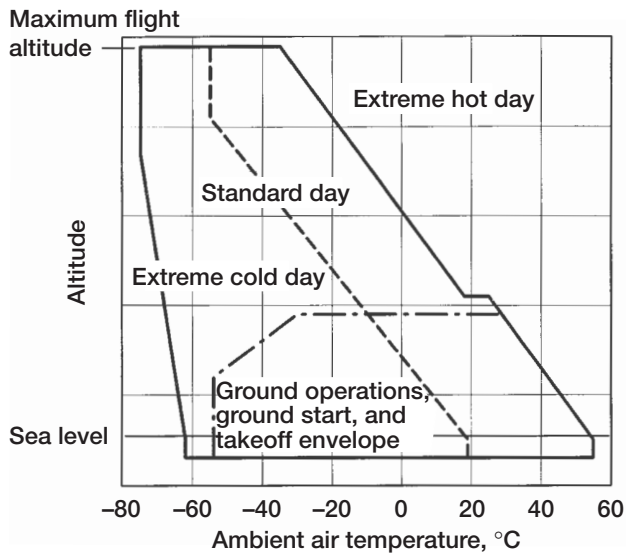


Figure 43.—Engine operating envelope. (Stoner, 1998.)
 Courtesy Pratt & Whitney.

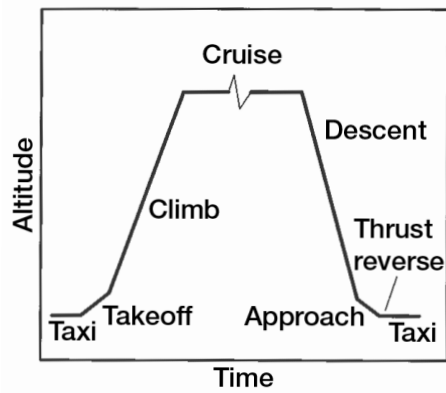


Figure 44.—Flight profile. (Stoner, 1998.)
 Courtesy Pratt & Whitney.

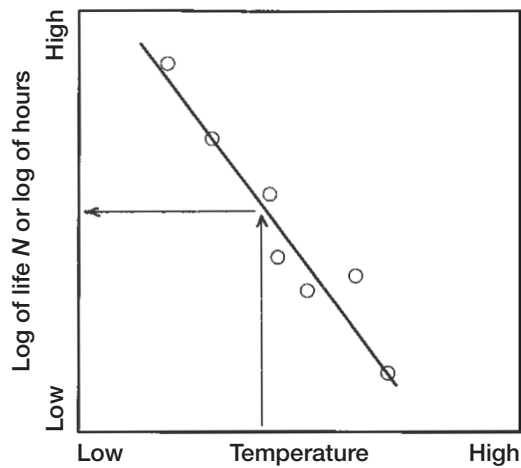


Figure 45.—Material life as function of temperature relation. (Stoner, 1998.)
 Courtesy Pratt & Whitney.

Aging of an engine usually contributes to increases in dynamic unbalance and forced vibrations of the externals and raises concern over harmonic resonance. Under dynamic test conditions the component is vibrated along three orthogonal axes at the four most significant resonances, where resonance is defined as an output/input ratio greater than 2. Input at a mounting point is usually 20 g's at frequencies to 3 kHz. The location of the gearbox on the case or fan represents a compromise of thermal demands (forward is cooler) and dynamic demands (rigidly mounted to hot case). In either case many brackets are required and many components and brackets experience infant mortality, which is totally unacceptable.

Although gas turbine engine externals are complex and perhaps more familiar, rocket engine externals are equally complex and require rigorous flight qualification acceptance testing prior to installation. Figure 46 features the main components of the space shuttle main engine (SSME) powerhead along with the low- and high-pressure oxygen turbopumps illustrated in the engine cutaway.^{3,4} This incredible liquid oxygen-hydrogen engine produces 512 950-lb thrust in the absence of an atmosphere (about 12.3 Mhp) at a vacuum specific impulse of 452 s, gobbling up nearly 516 kg/s (1135 lb/s) of propellant. Weighing in at 7480 lb the SSME has a dry thrust/weight ratio of 68.6. The thermomechanical extremes range from 20 K for the liquid hydrogen (LH₂) fuel system to 3590 K (6000 °F) combustor temperatures at 20.7 MPa (3000 psia) with a H₂/O₂ mixture ratio of 6:1. The liquid hydrogen turbomachine runs at 37 000 rpm, delivers 69 000 hp (400 hp/lb) at over 43 MPa (6230 psia) with millisecond response times. These machines represent significant sealing challenges. The liquid oxygen turbomachine runs at 27 000 rpm, delivers 25 000 hp at 29.6 MPa (4300 psia) with a preburner boost pump to over 50.5 MPa (7320 psia) with millisecond response. Under these conditions liquid oxygen is extremely hydrocarbon sensitive, and extreme care is taken to ensure hydrocarbon-free operation.

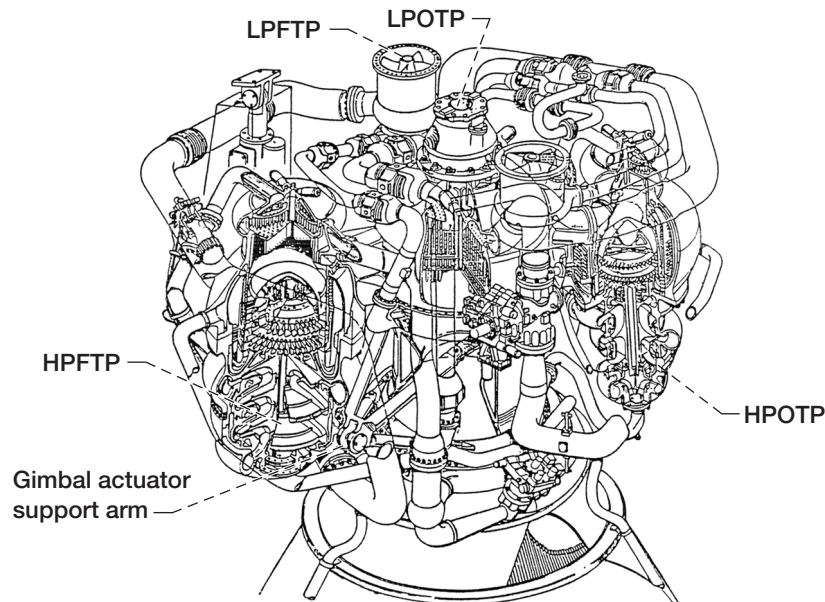


Figure 46.—Cutaway of space shuttle main engine (SSME) powerhead featuring high-pressure fuel turbopump (left) and high-pressure oxygen turbopump (right).

³In some engine circles the turbopumps are considered to be the rocket engine.

⁴Dynamics of the SSME turbopump are discussed in part 2.

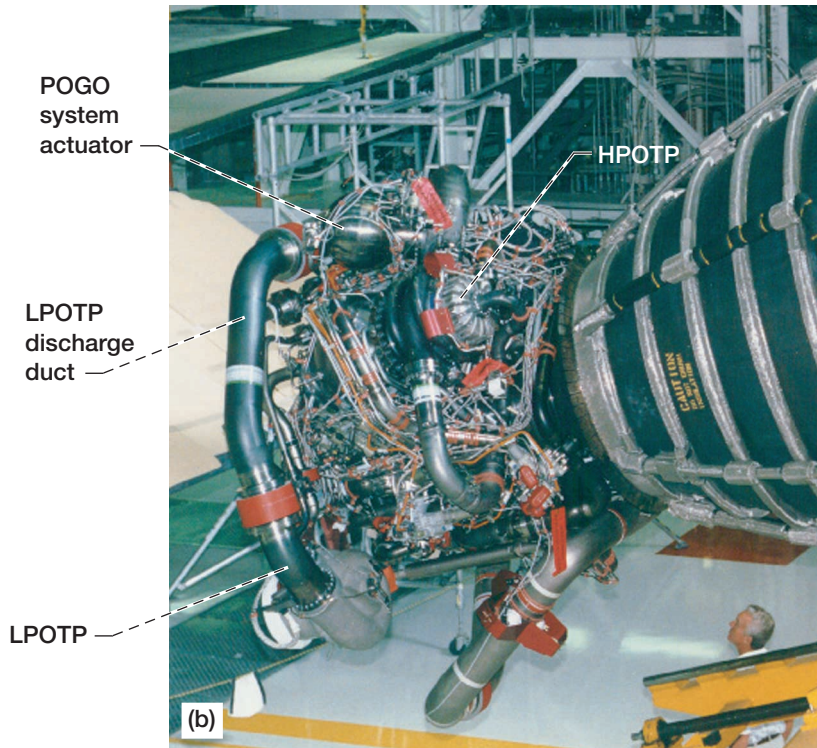
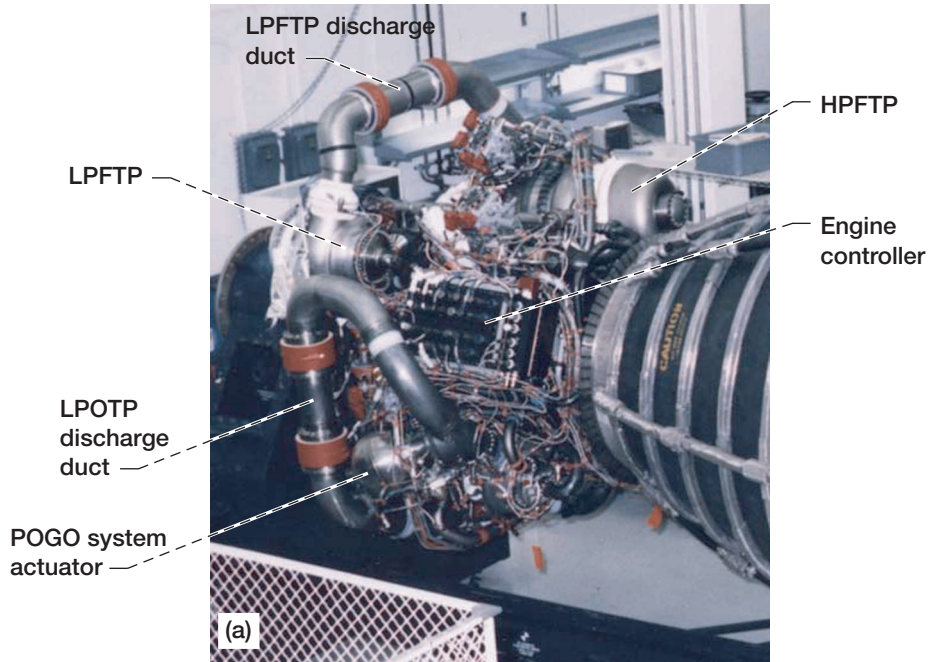


Figure 47.—Space shuttle main engine (SSME). (a) Engine externals featuring low- and high-pressure fuel turbopumps, transfer lines, and low-pressure oxidizer turbopump. [Stennis Space Center 94-006-1.jpg; <http://nix2.larc.nasa.gov/nix.html> (search on, Space Shuttle Main Engine Processing)]. (b) Engine ready for mating to orbiter (red flags are check points and also externals features). [<http://science.ksc.nasa.gov/shuttle/photos/>]. (c) Engine in process of mating with orbiter. [<http://science.ksc.nasa.gov/shuttle/photos/>].



Figure 47.—Concluded. (c) Engine in the process of mating with orbiter. [<http://science.ksc.nasa.gov/shuttle/photos/>].

The major differences between a rocket engine and a jet engine include the rocket engine's short operational times, low number of engine cycles, rapid start-stop characteristics with high power density, and high propellant flows. Also the rocket engine has its own oxidizer (cryogenic oxygen) and uses high-performance fuel (cryogenic hydrogen) at extreme thrust and operating conditions (sea level to orbit). In order to achieve these objectives, a myriad of externals (e.g., pipes, wires, valves, seals, instrumentation, controls, and brackets) are required for the engine to function safely and reliably (fig. 47). The handling, installation, and operational prowess of the SSME is simply staggering. Figures 47(b) and (c) illustrate the SSME engine being mated to the orbiter from the oxidizer and fuel turbopump sides and can be compared with figures 41 and 35 for the aeronautical turbomachines. In each orientation, for both engines, engine externals that support and sustain engine operation encompass all that Miller and Stoner define but are the least understood and researched from a systems point of view until a failure occurs. Then externals receive the attention they deserve.

Additional complexities such as interactive dynamics of the propellant lines, vehicle, and engines (e.g., POGO in rocket engines⁵ and inlet stall in aeronautical engines) are beyond the scope of this report but can shut the system down.

⁵POGO: A problem involving interactive dynamics of vehicle structure and propellant in the feedline column and the engine—analogous to a child on a pogo stick (Fenwick, 1992). Upward engine thrust (g-load) increases turbopump propellant inlet pressure causing additional propellant flow into the engine, which produces an additional upward force with a time delay. If the engine upward force is greater than the downward force at the engine propellant inlet, the engine acts like negative structural damping with potential for POGO. Anti-POGO systems may also require frequency matching or tuning of the feed system resonance with a structural resonance. In flight tuning and detuning occur naturally as propellant is consumed, potentially a transient phenomenon. The SSME-POGO suppressor, about the size of a basketball, is teed off the main liquid-oxygen duct just upstream of the high-pressure oxidizer turbopump. A mixture of gaseous oxygen at 478 K (440 °F) and liquid oxygen at 89 K (–300 °F) is continuously bled from the suppressor to control the gas volume and thereby the feed system dynamics, preventing POGO. Then the mixture is reintroduced into the feed line upstream of the engine so that all the “gas condenses” (Fenwick, 1992).

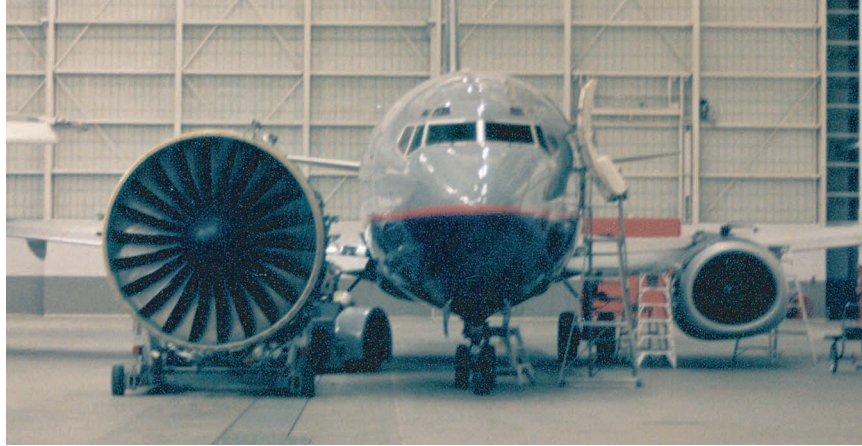


Figure 48.—Relative size of PW-4090 engine to Boeing 737 aircraft fuselage.
Courtesy United Airlines.

From figure 47 one begins to appreciate the relative size of the SSME and the space shuttle orbiter, yet another impressive comparison is between today's high-bypass engines that power the Boeing 777 aircraft. Figure 48 illustrates the relative size of a PW-4090 engine and a Boeing 737 aircraft; the engine diameter is nearly the same size as the 737-fuselage.

As can be realized, engine externals include the long lengths of static sealing as well as dynamic components that all must function efficiently with a high degree of reliability in order for the engine to run. So we now turn our attention to component and engine reliability.

Life and Reliability Issues

System design conditions for component cooling are driven by two similar but unique considerations: (1) compliance to Federal Aviation Administration (FAA) certification issues addressing safety and (2) FAA airworthiness regulations and component reliability (Dunkelberg, 1998). The mean time between failures is highly dependent on the thermal loading of components within the engine nacelle (fig. 49). The certification flight exposes the engine externals' cooling to a worst-case mixture of ambient temperature, engine power, and flight profile. It is indeed a stringent "wringing out" of the aircraft (fig. 50). This test represents a higher thermal environment than anticipated for the aircraft in revenue service, a once-in-a-lifetime, worst-case scenario. Although not governed by the FAA, the flight qualification of a space shuttle component is even more challenging. For example, each engine has over 50 000 components with more than 7000 tracked for periodic replacement. Nevertheless, the SSME has a demonstrated reliability of over 0.999. However, even though operational and healthy, it is still an experimental vehicle, and our recent loss emphasizes its vulnerability.

For aircraft engine life modeling the component environmental temperature calculation is based on 84 percent standard day, 15 percent maximum hot day, and 1 percent cold day conditions. For engine component life modeling the time τ_i and the life L_i under thermomechanical load from the environmental temperature and flight envelope is used to determine the cumulative loss of component life according to the linear damage rule of Palmgren, Langer, and Miner.

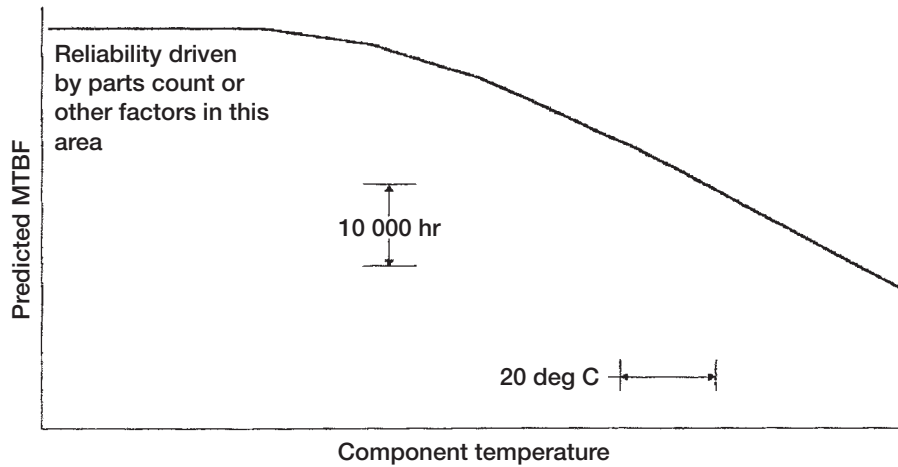


Figure 49.—Effect of component temperature on predicted mean time between failures for typical engine-mounted electronic device. (Dunkelberg, 1998.) Courtesy The Boeing Company.

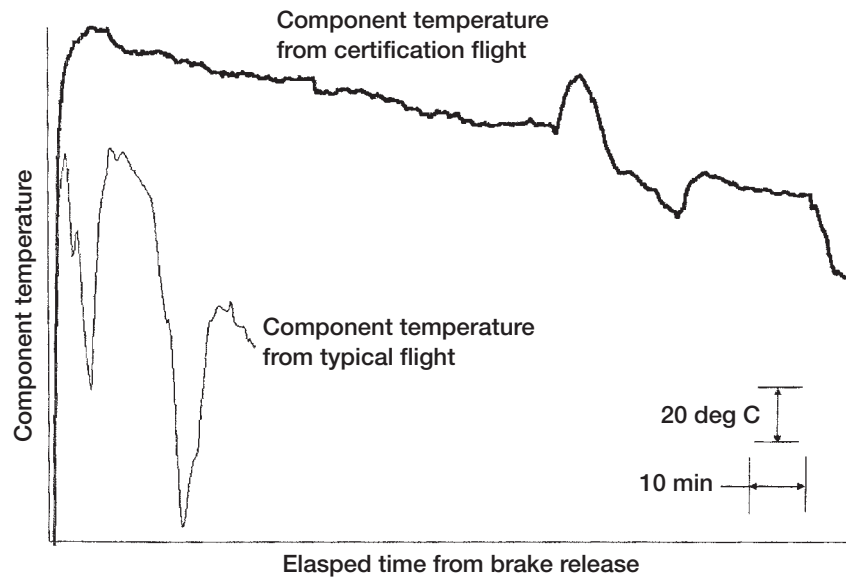


Figure 50.—Temperature of engine-mounted component for certification cooling climb and typical revenue climb corrected to hot day. (Dunkelberg, 1998.) Courtesy The Boeing Company.

$$R = \sum_{i=1}^m \tau_i / L_i \quad \text{and} \quad \text{Life} = \sum_{i=1}^m \tau_i / R \quad \text{where } 0 < R \leq 1 \quad (1)$$

For example, material spends 500 hr at 200 °C (390 °F), point τ_1, T_1 , and 300 hr at 250 °C (450 °F), point τ_2, T_2 . From the material-temperature-life curve (such as fig. 45) at 200 °C the life is 1000 hr (L_1, T_1) and at 250 °C the life is 600 hr (L_2, T_2).

$$R = 500/1000 + 300/600 = 5/6 \quad \text{and} \quad \text{Life} = (1000 + 300)/(5/6) = 1560 \text{ hr}$$

Under these conditions 5/6 of the material life is consumed in 1560 hr. If this is unsatisfactory, one must redesign. This method can sometimes be extended to the components. For ETOPS the components must pass a 3000-cycle engine test and a 1000-cycle flight test, where one cycle is an excursion between idle and high power.

Zaretsky et al. (2002) applied Weibull-based life and reliability analysis, based on the NASA E³ engine, to rotating engine structures. When limits are placed on stress, temperature, and time for a component's design, the criterion that will define the component's life and thus the engine's life will be either high-cycle or low-cycle fatigue. From the engine manufacturer's original component life calculations, the engine's life and reliability were determined on the basis of assumed values of each component's cumulative life distributions S as represented by a Weibull slope m and characteristic life X_β , where S is the probability of survival ($0 < S \leq 1$) at load cycle X .

$$\ln \ln \frac{1}{S} = m \ln \left[\frac{X}{X_\beta} \right] \quad (2)$$

The lives of the HPT disks and blades were also evaluated as a system and individually, where L_{sys} is the system life where components $L_1 \dots L_n$ are load cycled $X_1 \dots X_n$.

$$\frac{1}{L_{\text{sys}}} = \frac{X_1}{L_1} + \frac{X_2}{L_2} + \dots + \frac{X_n}{L_n} \quad (3)$$

and for components all having the same Weibull slope m ,

$$\frac{1}{L_{\text{sys}}^m} = \frac{1}{L_1^m} + \frac{1}{L_2^m} + \dots + \frac{1}{L_n^m} \quad (4)$$

Engine Life

Knowing the cumulative statistical distribution (Weibull function) of each engine component is a prerequisite to accurately predicting the life and reliability of an entire engine. As the engine Weibull slope increases, the predicted lives decrease. When using table I and equation (5) with $m_i = 3, 6, 9$ ($i = 1, 3$), the predicted engine lives L_5 (50 failures in 1000 engines in service) are approximately 17 000 and 32 000 hr, which depend on the assumed Weibull slope. These lives correlate with current engine maintenance practices without and with refurbishment, respectively. That is, it can be reasonably anticipated that at one of these time intervals 5 percent of the engines in service will have been removed for repair or refurbishment for cause.

$$\frac{1}{L_{\text{sys}}^{m_{\text{sys}}}} = \frac{1}{L_{\text{HPTBlade}}^{m_1}} + \frac{1}{L_{\text{HPT ROT. ST.}}^{m_2}} + \frac{1}{L_{\text{RE}}^{m_3}} \quad (5)$$

Blade Life

When using equation (6) and table II, the individual HPT blade lives necessary to obtain a blade system life $L_{0.1}$ (one failure in 1000 engines in service) of 9000 hr for Weibull slopes of 3, 6, and 9 are 47 391, 20 652, and 15 658 hr, respectively, for a system with $n = 146$ components.

$$L_{\text{blade}} = \left(n L_{\text{sys}}^m \right)^{(1/m)} = \left(146 \times 9000^m \right)^{(1/m)} \quad (6)$$

TABLE II.—E³-ENGINE FLIGHT PROPULSION SYSTEM
LIFE BASED ON 1985 TECHNOLOGY AND EXPERIENCE
[From Davis and Stearns, 1985.]

	Service life, hr	Total life with repair, hr
Combustor	9 000	18 000
HPT rotating structure	18 000	36 000
HPT blading	9 000	18 000
Remainder of engine	-----	36 000

Using these individual HPT blade lives (47 391, 20 652, and 15 658 hr), the values for X_β are found from equation (1) with $S = 0.999$. Knowing X_β , the probability of an individual blade retirement time X of 18 000 hr, constituting the entire blade life with repair, can then be found from equation (2). Then, reapplying equation (2), X of 18 000 hr can be found. For 1000 engines or 146 000 blades in service it would be expected that 8, 64, or 512 blades would be removed for cause prior to this time for Weibull slopes of 3, 6, or 9, respectively.

Turbine Examples

For a design life for each of the two HPT disks having probable points of failure equal to or greater than 36 000 hr at a probability of survival of 99.9 percent, the predicted disk system life $L_{0.1}$ can vary from 9408 to 24 911 hr depending on the Weibull slope (3, 6, or 9) assumed. The tabulated stress life data of Halila et al. (1982) were used for each disk, and the cross sections were assumed to repeat at 15° segments.

Liu (2001) cites thermomechanical cracking of steam turbine rotors at critical locations as causes of rotor instability that can lead to failure. He suggests that the rotor life limit be set at $0.7L_{\text{creep+fatigue}}$, whereupon shaft dynamics are monitored for crack initiation and propagation. No data are provided.

Need for Data

Within the open literature there is a dearth of data for critical engine components (HPT disk) and for basic materials. The classic approach to component and engine design has been deterministic. The deterministic method assumes that full and certain knowledge exists for the service conditions and

the material strength. Specific equations define an engine's operating condition and are coupled with experience-based safety factors. Variations with loading, such as platform and disk temperature and thermal gradients, can have a significant effect on component reliability. The Weibull-based analysis addresses these issues of component life and reliability (Zaretsky et al., 2002).

Summary

Altering engine sealing, particularly on the high-pressure spool or high-pressure pumps of the system, alters the entire engine dynamics. Knowing how to utilize these changes becomes a company's competitive edge. Cavity sealing of a turbomachine pump, compressor, or turbine is complex and has a significant effect on component and engine performance. Several numerical tools (e.g., NASA-developed INDSEAL, SCISEAL, and ADPAC) are available to help guide the designer and experimenter. And in time data will emerge to more rigorously validate these codes, from rig experiments to results from field operations. Now, however, the numerical tools cited are applicable, but the validation data are sparse.

As interesting as cavity, rim, platform, and tip flows are, most design codes find it necessary to minimize computations and represent these complex flow passages with simple models. The cost and complexity of including local geometric details necessary to capture these flows for a fan, compressor, or turbine become prohibitive. Nevertheless, in the details are challenges and opportunities for engine performance improvements. However, most funding and experiments are in support of design code validation and implementation.

Gas turbine engine externals inhabit the space between the engine case and the nacelle cowling. Rocket engine externals occupy a similar space within the confines of the aft-fairing frame. Within that space, overflowing with pipes, wires, and fire-extinguishing components, are challenges and opportunities for sealing long lengths of cowling and improving flow dynamics, cooling and fluid distribution, and dynamic components. All must function efficiently with a high degree of reliability in order for the engine to run.

Within the open literature there is a dearth of statistically significant data for critical engine components (e.g., the high-pressure turbine disk) and for basic materials. The classic approach to component and engine design has been deterministic. The deterministic method assumes that full and certain knowledge exists for the service conditions and the material strength. Specific equations define an engine's operating condition and are coupled with experience-based safety factors. In the "hands" of an experienced and seasoned designer or engineer, these equations are adequate. However, variations with loading can have a significant effect on component reliability. Stoner and Zaretsky addressed the reliability issues with Weibull-based analysis potentially applicable to the engine, but without validation data they are just studies. These variations and deficits in statistical databases require immediate attention.

References

- Adamczyk, J.J., Celestina, M.L., and Greitzer, E.M. (1993) The Role of Tip Clearance in High-Speed Fan Stall, *J. Turbomachinery*, vol. 115, no. 1, pp. 29–39.
- Allcock, D.C.J., Ivey, P.C., and Turner, J.R. (2002) Abradable Stator Gas Turbine Labyrinth Seals: Part 2, Numerical Modeling of Differing Seal Geometries and the Construction of a Second Generation Design Tool. AIAA Paper 2002–3937.

Ameri, A.A., Steinthorsson, E., and Rigby, D.L. (1999) Effects of Tip Clearance and Casing Recess on Heat Transfer and Stage Efficiency in Axial Turbines. Transactions ASME, Journal of Turbomachinery, Vol. 121, Oct., pp. 683–693.

Ameri, A.A. and Bunker (2000) Heat Transfer and Flow on the First-Stage Blade Tip of a Power Generation Gas Turbine: Part 2 Simulation Results, Transactions ASME, Journal of Turbomachinery, Vol. 122, April, pp. 272–277.

Athavale, M.M., Przekwas, A.J., and Hendricks, R.C. (1992) A Numerical Study of the Flow-Field in Enclosed Turbine Disk-Cavities in Gas Turbine Engines, Proceedings of the 4th International Symposium on Transport Phenomena and Dynamics of Rotating Machinery (ISROMAC-4).

Athavale, M.M., Przekwas, A.J., and Hendricks, R.C. (1993) Driven Cavity Simulation of Turbomachine Blade Flows With Vortex Control, AIAA Paper 93-0390.

Athavale, M.M., Przekwas, A.J., Hendricks, R.C., and Steinetz, B.M. (1995) Numerical Analysis of Intra-Cavity and Power-Stream Flow Interaction in Multiple Gas-Turbine Disk-Cavities, ASME Paper 95-GT-325.

Athavale, M.M., Przekwas, A.J., Hendricks, R.C., and Steinetz, B.M. (1997) Development of a Coupled, Transient Simulation Methodology for Interaction Between Primary and Secondary Flowpaths in Gas Turbine Engines, AIAA Paper 97-2727.

Athavale, M.M., Przekwas, A.J., Hendricks, R.C., and Steinetz, B.M. (1998) Coupled Transient Simulations of the Interaction Between Power and Secondary Flowpaths in Gas Turbines, AIAA Paper 98-3290.

Athavale, M.M., Ho, Y.H., and Przekwas, A.J. (1999) Analysis of Coupled Seals, Secondary and Powerstream Flow Fields in Aircraft and Aerospace Turbomachines, Final Report, NASA Contract NAS3-27392, December.

Athavale, M.M., Steinetz, B.M., and Hendricks, R.C. (2001) Gas Turbine Primary-Secondary Flow Path Interaction: Transient, Coupled Simulation and Comparison With Experiments, AIAA Paper 2001-3627.

Bilwakesh, K.R. and Koch, C.C. (1972) Evaluation of Range and Distortion Tolerance for High Mach Number Transonic Fan Stages, Task 2: Performance of a 1500-Foot-Per-Second Tip Speed Transonic Fan Stage With Variable Geometry Inlet Guide Vanes and Stator, NASA CR-72880.

Campbell, D.A. (1978) Gas Turbine Disk Sealing System Design, AGARD-CP-237 (AGARD-AR-123), Paper 18.

Chen, J.P. (1991) Unsteady Three-Dimensional Thin-Layer Navier-Stokes Solutions for Turbomachinery in Transonic Flows, Ph.D. Thesis, Department of Aerospace Engineering, Mississippi State University, Dec.

Chew, J.W. (1988) Predictions of Flow in Rotating Disk Systems Using the k - ϵ Turbulence Model, ASME Paper 88-GT-229.

Chew, J.W., Green, T., and Turner, A.B. (1992) Rim Sealing of Rotor-Stator Wheelspaces in the Presence of External Flow, *J. Turbomachinery*, vol. 114, pp. 426–432.

Copenhaver, W.W., Mayhew, E.R., Hah, C., and Wadia, A.R. (1996) The Effect of Tip Clearance on a Swept Transonic Compressor Rotor, *J. Turbomachinery*, vol. 118, Apr., pp. 230–239.

Davis, D.Y. and Stearns, E.M. (1985) Energy Efficient Engine Flight Propulsion System Final Design and Analysis, NASA CR–168219.

Dunkelberg, K. (1998) Commercial Airplane Nacelle Component (Engine Externals) Certification and Typical Temperature Exposure, Proceedings of the 7th International Symposium on Transport Phenomena and Dynamics of Rotating Machinery (ISROMAC–7). (See also NASA Advanced Subsonic Technology (AST) 028, 1998.)

Feiereisen, J.M., Paolillo, R.E., and Wagner, J. (2000) UTRC Turbine Rim Seal Ingestion and Platform Cooling Experiments, AIAA Paper 2000–3371, July.

Fenwick, J. (1992) POGO, Rocketdyne’s Engineering Journal of Power Technology, [http://www.engineering at boeing.com/articles/pogo.jsp](http://www.engineering.at.boeing.com/articles/pogo.jsp).

Ginn, K.B. (1998) An Experimental Approach for Engine Nacelle Flowfield Characterization, Proceedings of the 7th International Symposium on Transport Phenomena and Dynamics of Rotating Machinery (ISROMAC–7).

Graber, D.J., Daniels, W.A., and Johnson, B.V. (1987) Disk Pumping Test, AFWAL–TR–87–2050.

Halila, E.E., Lenahan, D.T., and Thomas, T.T. (1982) Energy Efficient Engine High Pressure Turbine Test Hardware: Detailed Design Report, NASA CR–167955.

Hall, E.J. and Delaney, R.A. (1993a) Investigation of Advanced Counterrotation Blade Configuration Concepts for High Speed Turboprop Systems, Task 5—Unsteady Counterrotation Ducted Propfan Analysis Computer Program User’s Manual, NASA CR–187125.

Hall, E.J. and Delaney, R.A. (1993b) Investigation of Advanced Counterrotation Blade Configuration Concepts for High Speed Turboprop Systems, Task 5—Unsteady Counterrotation Ducted Propfan Analysis Final Report, NASA CR–187126.

Hall, E.J. and Delaney, R.A. (1995) Investigation of Advanced Counterrotation Blade Configuration Concepts for High Speed Turboprop Systems, Task 7—ADPAC User’s Manual, NASA Contract NAS3–25270, NASA CR–195472.

Heidegger, N.J., Hall, E.J., and Delaney, R.A. (1996) Parameterized Study of High-Speed Compressor Seal Cavity Flow, NASA CR–198504. (Also AIAA Paper 96–2807, 1996.)

Hendricks, R.C., Steinetz, B.M., Athavale, M.M., Przekwas, A.J., Braun, M.J., Dozozo, M.I., Choy, F.K., Kudriavtsev, V.V., Mullen, R.L., and von Pragenau, G.L. (1995) Interactive Developments of Seals, Bearings, and Secondary Flow Systems With the Power Stream, *Int. J. Rotating Machinery*, vol. 1, no. 3–4, pp. 153–185.

Ho, Y.H., Athavale, M.M., Forry, J.M., Hendricks, R.C., and Steinetz, B.M. (1996) Numerical Simulation of Secondary Flow in Gas Turbine Disc Cavities, Including Conjugate Heat Transfer, ASME Paper 96-GT-67.

Janus, J.M. (1989) Advanced 3-D CFD Algorithm for Turbomachinery, Ph.D. Thesis, Department of Aerospace Engineering, Mississippi State University, May.

Janus, J.M. and Horstman, H.Z. (1992) Unsteady Flow-Field Simulation of Ducted Prop-Fan Configurations, AIAA Paper 92-0521.

Johnson, B.V., Daniels, W.A., Kaweki, E.J., and Martin, R.J. (1991) Compressor Drum Aerodynamic Experiments With Coolant Injected at Selected Locations, *J. Turbomachinery*, vol. 113, pp. 272-280.

Johnson, B.V., Mack, G.J., Paolillo, R.E., and Daniels, W.A. (1994) Turbine Rim Seal Gas Path Flow Ingestion Mechanisms, AIAA Paper 94-2703.

Johnsen, I.A. and Bullock, R.O., eds. (1965) Aerodynamic Design of Axial-Flow Compressors (Revised), NASA SP-36. (Supersedes declassified NACA Memorandums E56B03, E56B03a, and E56B03b, 1956.)

Lakshminarayana, B. (1996), *Fluid Dynamics and Heat Transfer of Turbomachinery*, John Wiley & Sons, New York.

Liu, K.M. (2001) Life Begins at 70, Proceedings of the 1st International Symposium on Stability Control of Rotating Machinery (ISCORMA-1).

Miller, M., Colehour, J., and Dunkelberg, K. (1998) Engine Case Externals, Challenges and Opportunities, Proceedings of the 7th International Symposium on Transport Phenomena and Dynamics of Rotating Machinery (ISROMAC-7). (See also NASA CP-10198, 1996.)

NASA Conference Publications—Hendricks, R.C., Liang, A.D., and Steinetz, B.M., eds., *Seals Code Development and Seal and Secondary Air Systems Workshops*, NASA CP-10124 (1992); NASA CP-10136 (1993); NASA CP-10181 (1995); NASA CP-10198 (1996); NASA CP-208916 (1998); NASA CP-210472 (2000); NASA CP-211208 (2001).

PDE: <http://www.grc.nasa.gov/WWW/AERO/base/pdet.htm>

Smout, P.D., Chew, J.W., and Childs, P.R.N. (2002) ICAS-GT: A European Collaborative Research Programme on Internal Cooling Air Systems for Gas Turbines, Paper GT-2002-30479.

Song, S.J. and Cho, S.H. (2000) Nonuniform Flow in a Compressor Due to Asymmetric Tip Clearance, *J. Turbomachinery*, vol. 122, Oct., pp. 751-760.

Stoner, B.L. (1998) The Importance of Engine Externals' Health, Proceedings of the 7th International Symposium on Transport Phenomena and Dynamics of Rotating Machinery (ISROMAC-7).

Strazisar, A.J., Wood, J.R., Hathaway, A.D., and Suder, K.L. (1989) Laser Anemometer Measurements in a Transonic Axial-Flow Fan Rotor, NASA TP-2879.

Strazisar, A.J. (1985) Investigation of Flow Phenomena in a Transonic Fan Rotor Using Laser Anemometry, *J. Engineering for Gas Turbine and Power*, vol. 107, Apr., pp. 427–435.

Teramachi, K., Manabe, T., Yanagidani, N., and Fujimura, T. (2002) Effect of Geometry and Fin Overlap on Sealing Performance of Rims Seals, *AIAA Paper 2002–3938*.

Van Zante, D.E., Stazisar, A.J., Wood, J.R., Hathaway, M.D., and Okiishi, T.H. (1999) Recommendations for Achieving Accurate Numerical Simulation of Tip Clearance Flows in Transonic Compressor Rotors, Paper 99–GT–390.

Virr, G.P., Chew, J.W., and Coupland, J. (1994) Application of Computational Fluid Dynamics to Turbine Disc Cavities, *J. Turbomachinery*, vol. 116, pp. 701–708.

Wellborn, S.R. and Okiishi, T.H. (1996) Effects of Shroud Stator Cavity Flows on Multistage Axial Compressor Performance, *NASA CR–198536*.

Wellborn, S.R. and Okiishi, T.H. (1999) The Influence of Shrouded Stator Cavity Flows on Multistage Compressor Performance, *J. Turbomachinery*, vol. 121, no. 3, pp. 486–498.

Wilson, J., Hendricks, R.C., Wu, T., and Flower, R. (1997) Bidirectional Brush Seals, *NASA TM–107351*. (<http://www.grc.nasa.gov/WWW/cdtb/projects/waverotor/index.html>).

Zaretsky, E.V., Hendricks, R.C., and Soditus, S. (2002) Weibull-Based Design Methodology for Rotating Aircraft Engine Structures, *Proceedings of the 9th International Symposium on Transport Phenomena and Dynamics of Rotating Machinery (ISROMAC–9)*.

Appendix—Symbols

Nomenclature for figures 24 to 34:

c	clearance gap
LE	leading edge
\dot{m}	mass flow rate
M	Mach number
P	pressure
PS	pressure side
SS	suction side
$r\omega$	rotor speed
r	rotor radius
t	blade thickness
T	temperature
TE	trailing edge
\vec{U}	rotor (moving coordinate) velocity ($V_\theta = r\omega$)
\vec{V}	absolute (stationary coordinate) velocity
\vec{V}_R	relative (moving coordinate) velocity
V_z	axial coordinate velocity
V_θ	circumferential coordinate velocity
Z	axial coordinate
θ	circumferential coordinate
ρ	fluid density

Subscripts:

L	low
H	high
s	static
t	total

Nomenclature for life and reliability issues:

$L_{0.1}$	1 failure in 1000 components
$L_{1, 2 \dots, n}$	life of components 1, 2 ..., n
L_5	50 failures in 1000 components
L_{blade}	blade life
L_i	life of material at temperature T_i based on test data
L_{sys}	system life based on $L_{1, 2 \dots, n}$
m	Weibull slope
n	number of system components
R	portion of life consumed at operating conditions
S	probability of survival
X	load cycles or time
X_β	Weibull characteristic life
τ_i	time spent at temperature T_i

Subscripts:

HPT Blade	high-pressure-turbine blade
HPT ROT.ST.	high-pressure rotating structure
RE	remainder of engine

REPORT DOCUMENTATION PAGE			<i>Form Approved</i> <i>OMB No. 0704-0188</i>	
Public reporting burden for this collection of information is estimated to average 1 hour per response, including the time for reviewing instructions, searching existing data sources, gathering and maintaining the data needed, and completing and reviewing the collection of information. Send comments regarding this burden estimate or any other aspect of this collection of information, including suggestions for reducing this burden, to Washington Headquarters Services, Directorate for Information Operations and Reports, 1215 Jefferson Davis Highway, Suite 1204, Arlington, VA 22202-4302, and to the Office of Management and Budget, Paperwork Reduction Project (0704-0188), Washington, DC 20503.				
1. AGENCY USE ONLY (Leave blank)		2. REPORT DATE July 2004	3. REPORT TYPE AND DATES COVERED Technical Memorandum	
4. TITLE AND SUBTITLE Turbomachine Sealing and Secondary Flows Part 3—Review of Power-Stream Support, Unsteady Flow Systems, Seal and Disk Cavity Flows, Engine Externals, and Life and Reliability Issues			5. FUNDING NUMBERS Cost Center 2250000013	
6. AUTHOR(S) R.C. Hendricks, B.M. Steinetz, E.V. Zaretsky, M.M. Athavale, and A.J. Przekwas				
7. PERFORMING ORGANIZATION NAME(S) AND ADDRESS(ES) National Aeronautics and Space Administration John H. Glenn Research Center at Lewis Field Cleveland, Ohio 44135-3191			8. PERFORMING ORGANIZATION REPORT NUMBER E-13662-3	
9. SPONSORING/MONITORING AGENCY NAME(S) AND ADDRESS(ES) National Aeronautics and Space Administration Washington, DC 20546-0001			10. SPONSORING/MONITORING AGENCY REPORT NUMBER NASA TM-2004-211991-PART3	
11. SUPPLEMENTARY NOTES Portions of this material were presented at the Second International Symposium on Stability Control of Rotating Machinery sponsored by Bently Pressurized Bearing Company, Gdansk, Poland, August 4-8, 2003. R.C. Hendricks, B.M. Steinetz, and E.V. Zaretsky, NASA Glenn Research Center; and M.M. Athavale and A.J. Przekwas, CFD Research Corporation, Huntsville, Alabama 35805. Responsible person, R.C. Hendricks, organization code 5000, 216-977-7507.				
12a. DISTRIBUTION/AVAILABILITY STATEMENT Unclassified - Unlimited Subject Categories: 01, 07, 20, and 37 Available electronically at http://gltrs.grc.nasa.gov This publication is available from the NASA Center for AeroSpace Information, 301-621-0390.			12b. DISTRIBUTION CODE	
13. ABSTRACT (Maximum 200 words) The issues and components supporting the engine power stream are reviewed. It is essential that companies pay close attention to engine sealing issues, particularly on the high-pressure spool or high-pressure pumps. Small changes in these systems are reflected throughout the entire engine. Although cavity, platform, and tip sealing are complex and have a significant effect on component and engine performance, computational tools (e.g., NASA-developed INDSEAL, SCISEAL, and ADPAC) are available to help guide the designer and the experimenter. Gas turbine engine and rocket engine externals must all function efficiently with a high degree of reliability in order for the engine to run but often receive little attention until they malfunction. Within the open literature statistically significant data for critical engine components are virtually nonexistent; the classic approach is deterministic. Studies show that variations with loading can have a significant effect on component performance and life. Without validation data they are just studies. These variations and deficits in statistical databases require immediate attention.				
14. SUBJECT TERMS Turbomachine; Seals; Secondary flow; Engine externals; Component life			15. NUMBER OF PAGES 53	
			16. PRICE CODE	
17. SECURITY CLASSIFICATION OF REPORT Unclassified	18. SECURITY CLASSIFICATION OF THIS PAGE Unclassified	19. SECURITY CLASSIFICATION OF ABSTRACT Unclassified	20. LIMITATION OF ABSTRACT	

